J Biol Inorg Chem
DOI 10.1007/s00775-016-1424-1

ORIGINAL PAPER

Synthesis of Ni(II) complexes bearing indole-based thiosemicarbazone ligands for interaction with biomolecules and some biological applications

Jebiti Haribabu[1] · Kumaramangalam Jeyalakshmi[1] · Yuvaraj Arun[2] · Nattamai S. P. Bhuvanesh[3] · Paramasivan Thirumalai Perumal[2] · Ramasamy Karvembu[1]

Received: 4 June 2016 / Accepted: 26 November 2016

Abstract A series of new Ni(II) complexes containing indole-based thiosemicarbazone ligands was synthesized and characterized by elemental analyses, and UV–visible, FT-IR, ^{1}H & ^{13}C NMR and mass spectroscopic techniques. The Ni(II) complexes (**1**–**4**) bear the general formula $[Ni\{C_{10}H_9N_2NHCSNH(R)\}_2]$ where R = hydrogen (**1**), 4-methyl (**2**), 4-phenyl (**3**) and 4-cyclohexyl (**4**). Molecular structure of ligands (L3 and L4) and complexes (**2**, **3** and **4**) was confirmed by single crystal X-ray crystallography. Four coordinated Ni(II) complexes showed square planar geometry. The interaction of the Ni(II) complexes with calf thymus DNA (CT-DNA) has been evaluated by absorption spectroscopic and ethidium bromide (EB) competitive binding studies, which revealed the intercalative interaction of the complexes with CT-DNA. Gel electrophoresis experiments showed the cleavage of DNA by the complexes without any external agent. Further, the interaction of the complexes with bovine serum albumin (BSA) was investigated using UV–visible, fluorescence and synchronous fluorescence spectroscopic methods, which showed that the complexes could bind strongly with BSA. Molecular docking was employed to understand the binding of the Ni(II) complexes with the molecular target B-DNA, human DNA topoisomerase I and BSA. All the Ni(II) complexes possess high antioxidant activity against 2-2-diphenyl-1-picrylhydrazyl (DPPH) radical and antihaemolytic activity. In addition, in vitro cytotoxicity of the Ni(II) complexes against lung cancer (A549), human breast cancer (MCF7) and mouse embryonic fibroblasts (L929) cell lines was investigated. Complex **4** has high cytotoxicity. The mode of cell death effected by complex **4** has been explored using Hoechst 33258 staining.

Graphical abstract Nickel(II) complexes of thiosemicarbazone ligands were synthesized and their DNA/protein binding, DNA cleavage and cytotoxicity abilities were studied.

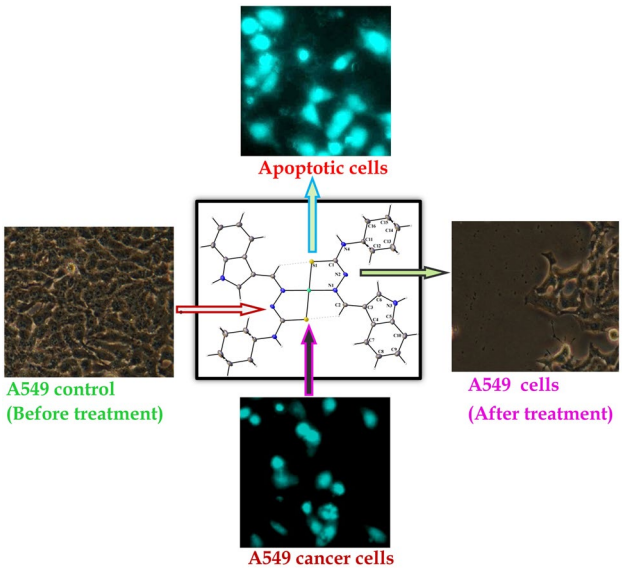

Keywords Indole · Thiosemicarbazones · Nickel(II) complexes · DNA/protein interactions · Cytotoxicity

Electronic supplementary material The online version of this article (doi:10.1007/s00775-016-1424-1) contains supplementary material, which is available to authorized users.

✉ Ramasamy Karvembu
kar@nitt.edu

[1] Department of Chemistry, National Institute of Technology, Tiruchirappalli 620015, India

[2] Organic Chemistry Division, CSIR-Central Leather Research Institute, Chennai 600020, India

[3] Department of Chemistry, Texas A&M University, College Station, TX 77842, USA

Published online: 19 December 2016

Introduction

Bioinorganic chemistry offers surplus opportunities for the design and making of pharmaceutical drugs that are not accessible to organic molecules [1–4]. Since the approval of cisplatin for the treatment of cancer, a number of other metal complexes has been investigated for their therapeutic potential [5, 6]. Among them, transition metal complexes of thiosemicarbazone ligands have received considerable interest due to their inhibition of DNA synthesis caused by a modification in the reductive conversion of ribonucleotides to deoxyribonucleotides [7]. In general, it has been observed that the biological activity of the complexes of thiosemicarbazones is greater than that of the corresponding free thiosemicarbazones [8–12]. Reactions of various thiosemicarbazones [7, 13–17] and semicarbazones [18] with diverse transition metal ions lead to the formation of metal complexes which have shown valuable biological activities. In particular, heterocyclic thiosemicarbazone complexes have aroused considerable interest in bioinorganic chemistry because of their pharmacological properties, particularly as antiphrastic, antibacterial, antioxidant and antitumoral agents [8, 19, 20]. For example, Ni(II) complexes with 6-methoxy-2-oxo-1,2-dihydroquinoline-3-carbaldehyde-based *N*-substituted thiosemicarbazones showed significant antioxidant and cytotoxicity [21].

Indole skeleton is present in the structure of many natural products with high structural complexities and biologically active molecules [22]. For this reason, indole and indole derivatives have been used, continuously, in different research areas such as pharmaceuticals, fragrances, agrochemicals, pigments and materials science [23]. One of the most important indole derivatives is an essential amino acid, tryptophan and it is one of the naturally occurring amino acids. Tryptophan-containing proteins have reducing effect on depression and insomnia related with hormonal fluctuations [24]. Research on indole-3-carbinol has been conducted using laboratory animals and cultured cells, which showed that it can prevent the binding of aflatoxin to DNA and hence it reduces the carcinogenic effects of aflatoxins [25–27]. Indole-3-carbinol was also effective in the prevention of breast and skin cancers [28, 29]. There are many drugs whose structures contain the indole nucleus, including sumatriptan, a tryptamine derivative [30] used in the treatment of migraine headaches, indomethacin and etodolac [31], which are used as non-steroidal anti-inflammatory drugs, and pindolol, a β-adrenoceptor antagonist [32]. These stem a great interest to develop indole-based thiosemicarbazone complexes for biological applications. Herein, we present the synthesis, structure, DNA binding, DNA cleavage, protein binding, DNA/protein molecular docking, antioxidant, antihaemolytic and cytotoxic studies of Ni(II) complexes containing indole-3-carbaldehyde-*N*-substituted thiosemicarbazones.

Experimental

General methods

All the chemicals were purchased from Sigma-Aldrich/Merck and used as received. Solvents were purified according to the standard procedures.

Physical measurements

Elemental analyses were done using a Vario EL-III CHNS analyser. FT-IR spectra were obtained as KBr pellets using a Nicolet-iS5 spectrophotometer. UV–visible spectra were recorded using a Shimadzu-2600 spectrophotometer. Emission spectral studies were carried out with a Jasco V-630 spectrophotometer using 5% DMF in buffer as the solvent. ^{1}H and ^{13}C NMR spectra were recorded on a Bruker 400 and 100 MHz spectrometer, respectively. MS–ESI spectra were recorded using a high-resolution JEOL and Q-Tof mass spectrometer.

Synthesis of thiosemicarbazones (L1–L4)

3-Indole aldehyde and the substituted thiosemicarbazide were combined (1:1) in ethanol (15 mL) in the presence of acetic acid (1–2 drops). The mixture was refluxed for 3 h, during which a white precipitate appeared. Then, the mixture was allowed to cool to room temperature and solid was filtered off. The product was washed with cold ethanol and purified by recrystallization from a methanol–dichloromethane mixture (1:2). The compounds were subsequently crystallized from acetonitrile–methanol mixture (1:1).

(*E*)-2-((1H-indol-3-yl)methylene) hydrazinecarbothioamide (L1)

Thiosemicarbazide (0.091 g, 0.001 mol) and 3-indole aldehyde (0.145 g, 0.001 mol) were used. Yield: 91%. White. m.p.: 162 °C. Anal. Calc. for $C_{10}H_{10}N_4S$ (%): C, 55.02; H, 4.62; N, 25.67; S, 14.69. Found: C, 55.27; H, 4.73; N, 25.26; S, 14.80. UV–Vis (CH_3OH): λ_{max}, nm 264, 330. FT-IR (KBr): υ, cm $^{-1}$ 3448 (N–H), 3312, 3230 (H–N–C=S), 1548 (C=N), 1295 (C=S). ^{1}H NMR (400 MHz, DMSO-d_6): δ, ppm 11.61 (s, 1H), 11.19 (s, 1H), 8.30 (s, 1H), 8.22 (d, J = 7.6 Hz, 1H), 8.02 (s, 1H), 7.80 (s, 1H), 7.43 (d, J = 7.2 Hz, 2H), 7.20 (t, J = 7.6 Hz, 1H), 7.13 (t, J = 7.6 Hz, 1H). ^{13}C NMR (100 MHz, DMSO-d_6): δ, ppm 176.8 (C=S), 141.4 (C=N), 137.4, 131.4, 124.3, 123.1,

122.5, 121.1, 112.2, 111.5 (aromatic C). TOF–MS–ES+: *m/z* [Found (Calcd)] 219.0713 (218.0626) $(M + H)^+$.

(*E*)-2-((1H-indol-3-yl) methylene)-*N*-methylhydrazinecarbothioamide (L2)

4-Methyl thiosemicarbazide (0.105 g, 0.001 mol) and 3-indole aldehyde (0.145 g, 0.001 mol) were used. Yield: 85%. White. m.p.: 154 °C. Anal. Calc. for $C_{11}H_{12}N_4S$ (%): C, 56.87; H, 5.21; N, 24.12; S, 13.80. Found: C, 56.94; H, 5.32; N, 24.0; S, 13.91. UV–Vis (CH_3OH): λ_{max}, nm 262, 329. FT-IR (KBr): υ, cm^{-1} 3440 (N–H), 3325, 3238 (H–N–C=S), 1551 (C=N), 1299 (C=S). ^{1}H NMR (400 MHz, DMSO-d_6): δ, ppm 11.61 (s, 1H), 11.18 (s, 1H), 8.29 (d, $J = 11.6$ Hz, 2H), 7.92 (d, $J = 4.0$ Hz, 1H), 7.80 (s, 1H), 7.43 (d, $J = 7.6$ Hz, 1H), 7.21 (t, $J = 7.6$ Hz, 1H), 7.15 (t, $J = 7.2$ Hz, 1H), 3.08 (d, $J = 4.0$ Hz, 1H). ^{13}C NMR (100 MHz, DMSO-d_6): δ, ppm 177.1 (C=S), 140.9 (C=N), 137.4, 131.3, 124.3, 123.1, 122.7, 121.0, 112.2, 111.6 (aromatic C), 31.5 (aliphatic C). TOF–MS–ES+: *m/z* [Found (Calcd)] 233.0862 (232.0783) $(M + H)^+$.

(*E*)-2-((1H-indol-3-yl) methylene)-*N*-phenylhydrazinecarbothioamide (L3)

4-Phenyl thiosemicarbazide (0.167 g, 0.001 mol) and 3-indole aldehyde (0.145 g, 0.001 mol) were used. Yield: 89%. White. m.p.: 170 °C. Anal. Calc. for $C_{16}H_{14}N_4S$ (%): C, 65.28; H, 4.79; N, 19.03; S, 10.89. Found: C, 65.41; H, 4.65; N, 19.37; S, 10.94. UV–Vis (CH_3OH): λ_{max}, nm 265, 341. FT-IR (KBr): υ, cm^{-1} 3453 (N–H), 3300, 3169 (H–N–C=S), 1549 (C=N), 1287 (C=S). ^{1}H NMR (400 MHz, DMSO-d_6): δ, ppm 11.72 (s, 1H), 11.63 (s, 1H), 9.65 (s, 1H), 8.46 (s, 1H), 8.27 (d, $J = 7.6$ Hz, 1H), 7.92 (s, 1H), 7.67 (d, $J = 8.0$ Hz, 2H), 7.48 (d, $J = 8.0$ Hz, 1H), 7.39 (d, $J = 7.6$ Hz, 2H), 7.25–7.16 (m, 3H). ^{13}C NMR (100 MHz, DMSO-d_6): δ, ppm 174.9 (C=S), 141.8 (C=N), 139.7, 137.5, 131.7, 128.6, 125.5, 125.4, 124.5, 123.2, 122.2, 121.2, 112.4, 111.4 (aromatic C). TOF–MS–ES+: *m/z* [Found (Calcd)] 295.1005 (294.0936) $(M + H)^+$.

(*E*)-2-((1H-indol-3-yl) methylene)-*N*-cyclohexylhydrazinecarbothioamide (L4)

4-Cyclohexyl thiosemicarbazide (0.173 g, 0.001 mol) and 3-indole aldehyde (0.145 g, 0.001 mol) were used. Yield: 89%. White. m.p.: 179 °C. Anal. Calc. for $C_{16}H_{20}N_4S$ (%): C, 63.97; H, 6.71; N, 18.65; S, 10.67. Found: C, 64.37; H, 6.43; N, 18.86; S, 10.90. UV–Vis (CH_3OH): λ_{max}, nm 264, 331. FT-IR (KBr): υ, cm^{-1} 3425 (N–H), 3343, 3241 (H–N–C=S), 1567 (C=N), 1291 (C=S). ^{1}H NMR (400 MHz, $CDCl_3$): δ, ppm 11.64 (s, 1H), 11.21 (s, 1H), 9.72 (s, 1H), 8.76 (s, 1H), 8.06 (d, $J = 8.0$ Hz, 1H), 8.04 (s, 1H), 7.44 (d, $J = 8.0$ Hz, 1H), 7.38 (d, $J = 8.0$ Hz, 1H), 7.32–7.24 (m, 2H), 4.33 (t, $J = 4.0$ Hz, 1H), 2.14 (t, $J = 12.0$ Hz, 2H), 1.80–1.63 (m, 4H), 1.51–1.28 (m, 4H). ^{13}C NMR (100 MHz, $CDCl_3$): δ, ppm 174.9 (C=S), 139.3 (C=N), 136.9, 129.1, 124.2, 123.7, 121.6, 121.5, 112.2, 111.7 (aromatic C), 52.6, 32.8, 29.7, 25.5, 24.6, 14.1 (aliphatic C). TOF–MS–ES+: *m/z* [Found (Calcd)] 301.1478 (300.1409) $(M + H)^+$.

Synthesis of Ni(II) complexes (1–4)

The ethanolic solution of $NiCl_2{\cdot}6H_2O$ (1 mmol) was added into the solution of an appropriate indole-based thiosemicarbazone ligand (1 mmol) in ethanol and a few drops of triethyl amine were added. The reaction mixture was stirred for 3 h under reflux, and then the precipitate formed was filtered and washed with ethanol. The suitable crystals for X-ray diffraction were grown from CH_2Cl_2–DMF mixture (2:1).

Bis[(*E*)-2-((1H-indol-3-yl)methylene) hydrazinecarbothioamide]Ni(II) (1)

$NiCl_2{\cdot}6H_2O$ (0.237 g, 0.001 mol) and L1 (0.218 g, 0.001 mol) were used. Yield: 87%. Light green solid. m.p.: 216 °C. Anal. Calcd. For $C_{20}H_{18}N_8NiS_2$: C, 48.70; H, 3.68; N, 22.72; S, 13.00. Found: C, 48.53; H, 3.40; N, 22.96; S, 13.14. UV–Vis (DMF): λ_{max}, nm 271, 334, 408. FT-IR (KBr): υ, cm^{-1} 3439, 3304 (N–H), 1502 (C=N), 1263 (C–S). ^{1}H NMR (400 MHz, DMSO-d_6): δ, ppm 11.99 (s, 1H), 8.64 (s, 1H), 7.61 (s, 1H), 7.51 (s, 1H), 7.46 (d, $J = 8.0$ Hz, 1H), 7.19 (t, $J = 7.6$ Hz, 2H), 6.92 (s, 1H). ^{13}C NMR (100 MHz, DMSO-d_6): δ, ppm 173.2 (C–S), 147.2 (C=N), 135.6, 134.4, 126.8, 122.9, 121.3, 117.1, 112.7, 109.6 (aromatic C). FT–MS–ESI+: *m/z* [Found (Calcd)] 493.0522 (492.0447) $(M + H)^+$.

Bis[(*E*)-2-((1H-indol-3-yl) methylene)-*N*-methylhydrazinecarbothioamide]Ni(II) (2)

$NiCl_2{\cdot}6H_2O$ (0.237 g, 0.001 mol) and L2 (0.232 g, 0.001 mol) were used. Yield: 80%. Light green solid. m.p.: 204 °C. Anal. Calcd. For $C_{22}H_{22}N_8NiS_2$: C, 50.69; H, 4.25; N, 21.50; S, 12.30. Found: C, 50.75; H, 4.08; N, 21.21; S, 12.48. UV–Vis (DMF): λ_{max}, nm 276, 380, 410. FT-IR (KBr): υ, cm^{-1} 3436, 3321 (N–H), 1509 (C=N), 1261 (C–S). ^{1}H NMR (400 MHz, DMSO-d_6): δ, ppm 11.92 (s, 1H), 8.40 (d, $J = 9.2$ Hz, 1H), 7.90 (d, $J = 8.0$ Hz, 1H), 7.83 (s, 1H), 7.45 (d, $J = 10.0$ Hz, 1H), 7.30–7.18 (m, 2H), 2.82 (s, 3H). ^{13}C NMR (100 MHz, DMSO-d_6): δ, ppm 173.6 (C–S), 141.6 (C=N), 135.4, 133.9, 126.8, 123.1, 121.4, 117.2, 112.8, 109.7 (aromatic C), 32.3 (aliphatic C).

FT–MS–ESI+: *m/z* [Found (Calcd)] 521.0835 (520.0762) $(M + H)^+$.

Bis[(*E*)-2-((1H-indol-3-yl) methylene)-*N*-phenylhydrazinecarbothioamide]Ni(II) (3)

$NiCl_2{\cdot}6H_2O$ (0.237 g, 0.001 mol) and L3 (0.294 g, 0.001 mol) were used. Yield: 83%. Light green solid. m.p.: 237 °C. Anal. Calcd. For $C_{32}H_{26}N_8NiS_2$: C, 59.55; H, 4.06; N, 17.36; S, 9.94. Found: C, 59.32; H, 4.19; N, 17.11; S, 10.03. UV–Vis (DMF): λ_{max}, nm 284, 392, 416. FT-IR (KBr): υ, cm^{-1} 3437, 3304 (N–H), 1500 (C=N), 1243(C–S). ^{1}H NMR (400 MHz, DMSO-d_6): δ, ppm 12.17 (s, 1H), 9.56 (s, 1H), 8.33 (s, 1H), 8.13 (d, $J = 7.2$ Hz, 1H) 7.81 (s, 1H), 7.55 (d, $J = 6.4$ Hz, 2H), 7.36 (t, $J = 6.4$ Hz, 1H), 7.27 (d, $J = 6.4$ Hz, 2H), 7.10–7.05 (m, 2H), 6.96 (t, $J = 6.4$ Hz, 1H). ^{13}C NMR (100 MHz, DMSO-d_6): δ, ppm 174.7 (C–S), 141.7 (C=N), 139.6, 137.4, 131.7, 128.5, 126.8, 125.4, 124.4, 123.0, 121.1, 120.4, 112.3, 110.2 (aromatic C). FT–MS–ESI+: *m/z* [Found (Calcd)] 645.1148 (644.1075) $(M + H)^+$.

Bis[(*E*)-2-((1H-indol-3-yl) methylene)-*N*-cyclohexylhydrazinecarbothioamide] Ni(II) (4)

$NiCl_2{\cdot}6H_2O$ (0.237 g, 0.001 mol) and L4 (0.300 g, 0.001 mol) were used. Yield: 86%. Light green solid. m.p.: 230 °C. Anal. Calcd. For $C_{32}H_{38}N_8NiS_2$: C, 58.45; H, 5.83; N, 17.04; S, 9.75. Found: C, 58.19; H, 5.92; N, 17.35; S, 9.61. UV–Vis (DMF): λ_{max}, nm 274, 328, 413. FT-IR (KBr): υ, cm^{-1} 3419, 3336 (N–H), 1511 (C=N), 1254 (C–S). ^{1}H NMR (400 MHz, DMSO-d_6): δ, ppm 12.05 (s, 1H), 8.39 (s, 1H), 7.68 (s, 1H), 7.54 (s, 1H), 7.47 (d, $J = 8.0$ Hz, 2H), 7.34 (s, 1H), 7.20 (t, $J = 6.8$ Hz, 2H), 2.01 (d, $J = 10.4$ Hz, 2H), 1.77 (d, $J = 11.6$ Hz, 2H), 1.62 (d, $J = 11.6$ Hz, 1H), 1.40–1.28 (m, 2H), 1.26–1.15 (m, 4H). ^{13}C NMR (100 MHz, DMSO-d_6): δ, ppm 174.0 (C–S), 141.1 (C=N), 135.5, 133.1, 126.8, 121.3, 117.2, 112.7, 109.8 (aromatic C), 79.6, 55.0, 32.5, 25.8, 25.4 (aliphatic C). FT–MS–ESI+: *m/z* [Found (Calcd)] 657.2087 (656.2014) $(M + H)^+$.

Single crystal X-ray crystallography

Single crystal X-ray diffraction data were collected using Bruker APEX2 (L4, **2**, **3** and **4**) and Bruker GADDS (L3) X-ray (three-circle) diffractometer. The X-ray radiation employed was generated from a Mo sealed X-ray tube ($K_\alpha = 0.70173$ Å) for the former and Cu sealed X-ray tube ($K_\alpha = 1.5418$ Å) fitted with a graphite monochromator in the parallel mode (175 mm collimator with 0.5 mm pinholes) for the latter. Sixty data frames were taken at widths of 0.5°. These reflections were used in the autoindexing procedure to determine the unit cell. A suitable cell was found and refined by nonlinear least squares and Bravais lattice procedures. Integrated intensity information for each reflection was obtained by reduction of data frames with APEX2 [33]. SADABS was employed to correct the data for absorption effects [34]. The structures were solved by direct methods SHELXTL (XS), and refined (SHELX-97, weighted least squares refinement on F^2) using APEX2 and OLEX2 [35, 36]. Hydrogen atoms were placed in idealized positions and were set riding on the respective parent atoms. All non-hydrogen atoms were refined with anisotropic thermal parameters. The structures were refined (weighted least squares on F^2) to convergence [35]. Olex2 was employed for the final data presentation and structure plots [36]. The crystallographic data and the results of refinements are summarized in Tables 1, 2, S1 and S2.

DNA binding experiments

For DNA absorption spectral studies, DNA samples were dissolved in 50 mM NaCl/5 mM Tris–HCl (pH 7.2) solution. CT-DNA solution displayed a UV absorbance ratio at 260 and 280 nm (*A*260/*A*280) of ca. 1.9:1, indicating that the CT-DNA was sufficiently in protein-free form [37]. The concentration of the nucleic acid solutions was determined by UV absorbance at 260 nm after 1:100 dilutions. The extinction coefficient at 260 nm was taken as 6600 M^{-1} cm^{-1} [38]. Stock solutions were stored at 4 °C and used within 4 days. Concentrated stock solutions were prepared by dissolving calculated amounts of the complexes (**1**, **2**, **3** and **4**) in a 5% DMF/5 mM Tris–HCl/50 mM NaCl buffer to required concentrations for all the experiments. Absorption spectral titration experiments were performed by maintaining a constant concentration of the complex and varying the nucleic acid concentration (0–35 μM). The spectra were recorded after equilibration for 3 min, allowing the compounds to bind to the CT-DNA.

The competitive studies of each complex with ethidium bromide (EB) have been investigated using fluorescence spectroscopic technique. The excitation wavelength was fixed, and emission range was adjusted before measurements. DNA was pretreated with EB in the 1:1 ratio for 15 min. The complexes were then added to this mixture, and their effect on the emission intensity was measured. The Stern–Volmer equation was used to evaluate the apparent binding constant (K_{app}) and quenching constant (K_q) values of the complexes. The changes in fluorescence intensities at 596 nm (510 nm excitation) of EB bound to DNA were recorded with an increasing amount of the complexes

Table 1 Crystallographic data and refinement parameters for complexes (**2**, **3** and **4**)

	2	**3**	**4**
Empirical formula	$C_{28}H_{36}N_{10}NiO_2S_2$	$C_{44}H_{54}N_{12}NiO_4S_2$	$C_{38}H_{52}N_{10}NiO_2S_2$
Formula weight	667.50	937.82	803.72
Temperature (K)	110.15	110.15	110.15
Wavelength (Å)	0.71073	0.71073	0.71073
Crystal system	Triclinic	Triclinic	Triclinic
Space group	*P-1*	*P-1*	*P-1*
Unit cell dimensions			
a (Å)	8.4986(17)	8.985(2)	8.187(3)
b (Å)	10.336(2)	10.067(3)	12.458(4)
c (Å)	10.454(2)	13.855(4)	19.638(7)
α (°)	62.048(2)	108.319(3)	88.627(4)
β (°)	70.741(2)	91.914(3)	78.777(4)
γ (°)	78.337(2)	104.849(3)	83.653(4)
Volume ($Å^3$)	764.5(3)	1141.0(5)	1952.5(12)
Z	1	1	2
Density (calculated) Mg/m^3	1.450	1.365	1.367
Absorption coefficient (mm^{-1})	0.816	0.573	0.652
F(000)	350	494	852
Crystal size (mm^3)	0.57 × 0.56 × 0.53	0.48 × 0.2 × 0.17	0.54 × 0.52 × 0.2
Theta range for data collection (°)	2.234–27.509	2.221–27.613	1.057–27.768
Index ranges	$-11 \le h \le 10$, $-13 \le k \le 13$, $-13 \le l \le 13$	$-11 \le h \le 11$, $-13 \le k \le 13$, $-18 \le l \le 17$	$-10 \le h \le 10$, $-16 \le k \le 16$, $0 \le l \le 25$
Reflections collected	8713	13209	8859
Independent reflections [R(int)]	3453 [0.0260]	5195 [0.0314]	8859
Completeness to theta = 25.24°/25.24°/25.24°	99.5%	99.5%	99.5%
Absorption correction	Semi-empirical from equivalents	Semi-empirical from equivalents	Semi-empirical from equivalents
Max. and min. transmission	0.7456 and 0.4507	0.7456 and 0.6258	0.746 and 0.456
Refinement method	Full-matrix least squares on F^2	Full-matrix least squares on F^2	Full-matrix least squares on F^2
Data/restraints/parameters	3453/0/200	5195/0/290	8859/8/501
Goodness-of-fit on F^2	1.053	1.031	1.046
Final *R* indices [$I > 2$ sigma(I)]	R1 = 0.0256, wR2 = 0.0644	R1 = 0.0391, wR2 = 0.0923	R1 = 0.0519, wR2 = 0.1291
R indices (all data)	R1 = 0.0268, wR2 = 0.0651	R1 = 0.0539, wR2 = 0.0996	R1 = 0.0733, wR2 = 0.1421
Extinction coefficient	0.108(4)	n/a	n/a
Largest diff. peak and hole ($e.Å^{-3}$)	0.501 and −0.325	0.608 and −0.301	0.633 and −0.636

until maximum reduction in the intensity of fluorescence occurred.

Viscosity experiments were carried out using a semi-microviscometer maintained at 27 °C in a thermostatic water bath. DNA samples (0.5 mM) were prepared by sonication to minimize complexities arising from DNA flexibility [39]. Flow time was measured three times for each sample and an average flow time was calculated. The values of relative specific viscosity (η/η^0), where η is the relative viscosity of DNA in the presence of the complex and η^0 is the relative viscosity of DNA alone, were plotted against 1/*R* (1/*R* = [compound]/[DNA]). Relative viscosity (η^0) values were calculated from the observed flow time of the DNA solution (t) corrected for the flow time of the buffer alone (t^0), using the expression $\eta^0 = (t - t^0)/t^0$ [40–42].

CD spectroscopic technique is useful in monitoring the conformational changes induced by the interaction of drugs with the DNA helix. The B-form conformation of DNA showed two consecutive CD bands in the UV region, a positive band at 275 nm is due to base stacking and a negative band at 245 nm is due to polynucleotide helicity. CD spectra of DNA in the absence and presence of the complexes was recorded with a J-715 spectropolarimeter (Jasco) at 25 °C with a 0.1 cm path length cuvette. The spectra were recorded for 20 μM of DNA in the absence and presence of 5 μM of the Ni(II) complexes (**1**–**4**) in the region 220–300 nm [43].

Table 2 Selected bond lengths (Å), angles (°) of **2**, **3** and **4**

	2	3	4
Ni(1)–S(1)#1	2.1683(5)	2.1764(6)	2.1618(10)
Ni(1)–S(1)	2.1683(5)	2.1764(6)	2.1618(10)
Ni(1)–N(1)	1.9087(11)	1.9068(16)	1.911(2)
Ni(1)–N(1)#1	1.9087(11)	1.9068(16)	1.911(2)
S(1)–Ni(1)–S(1)#1	180.0	180.0	180.0
N(1)#1–Ni(1)–S(1)#1	85.58(3)	85.46(5)	85.86(7)
N(1)–Ni(1)–S(1)#1	94.42(3)	94.54(5)	94.14(7)
N(1)–Ni(1)–S(1)	85.58(3)	85.46(5)	85.86(7)
N(1)#1–Ni(1)–S(1)	94.42(3)	94.54(5)	94.14(7)
N(1)#1–Ni(1)–N(1)	180.0	180.00(9)	180.0
C(10)–S(1)–Ni(1)	95.11(5)	95.24(7)	96.75(10)
N(2)–N(1)–Ni(1)	120.45(8)	120.69(12)	122.01(18)
C(1)–N(1)–Ni(1)	125.28(9)	125.33(13)	125.39(19)

Symmetry transformations used to generate equivalent atoms: #1 $-x+1, -y, -z+1$

DNA cleavage experiment

A mixture of Tris buffer (5 mM Tris–HCl/50 mM NaCl buffer, pH 7.2), pUC19 plasmid DNA (150 μg/mL) and different amounts of the complexes was incubated for 4 h at 37 °C. A dye solution (0.05% bromophenol blue and 5% glycerol) was added to the reaction mixture prior to electrophoresis. The samples were then analysed by 1.5% agarose gel electrophoresis [Tris HCl/Boric acid/EDTA (TBE) buffer, pH 8.0] for 3 h at 60 mV. The gel was stained with 0.5 μg mL^{-1} EB, visualized by UV light, and photographed. The extent of cleavage of the pUC19 DNA was determined by measuring the intensities of the bands using Alpha Imager HP instrument.

Protein binding experiment

Quenching of the emission of tryptophan residues of BSA was performed using the complexes as quenchers. To a solution of BSA in phosphate buffer (pH 7.2), increments of the quenchers were added, and the emission signal at 341 nm (280 nm excitation) was recorded after each addition of the quencher. The excitation and emission slit widths and scan rates were constantly maintained for all the experiments. Concentrated stock solutions of the test compounds were prepared by dissolving them in DMF and diluted suitably with phosphate buffer to get required concentrations. 2.5 mL of BSA solution (1 μM) was titrated by successive additions of a 5 mL of stock solution of the test compounds (10^{-4} M) using a micropipette. Synchronous fluorescence spectra were also recorded using the same concentration of BSA and the test compounds as mentioned above with two different Δλ (difference between the excitation and emission wavelengths of BSA) values such as 15 and 60 nm [44].

Molecular docking studies

The X-ray crystal structure of B-DNA (PDB ID: 1BNA), dodecamer $d(CGCGAATTCGCG)_2$ human DNA Topo-I complex (PDB ID: 1SC7) and BSA (PDB ID: 3V03) was obtained from the Protein Data Bank (http://www.rcsb.org/pdb). 2D structure of the Ni(II) complexes was drawn using Chem Draw Ultra 12.0 (ChemOffice 2010). Chem3D Ultra 12.0 was used to convert 2D structure into 3D and the energy was minimized using semi-empirical AM1 method. Molecular docking studies have been done using the AutoDock Tools (ADT) version 1.5.6 and Auto Dock version 4.2.5.1 docking program [45]. The energy calculations were made using genetic algorithms. The outputs were exported to PyMol for visual inspection of the binding modes and for possible polar and hydrophobic interactions of the complexes with DNA and BSA.

Antioxidant assay

The antioxidant activity of the Ni(II) complexes was evaluated using the DPPH free radical scavenging assay [46, 47]. 5 mg of the each compound was dissolved in 1 mL of DMSO, which was maintained as a stock solution. From the stock, 25, 50, 75, 100, 250 and 500 μg of solutions were prepared. For the positive control, ascorbic acid at different concentrations (25, 50, 75, 100, 250 and 500 μg) was used. 100 μL of DPPH (at 10 mM concentration) and 900 μL of methanol were added to different concentrations of the compounds and also to the positive control, to screen the antioxidant potential. 100 μL of DPPH was added to 100 μL of DMSO and 900 μL of methanol to reveal the scavenging effect of DMSO. 1 mL of methanol was added to 100 μL of DPPH, which was used as a negative control. The mixtures were shaken vigorously and allowed to stand for 30 min in dark, which were analysed for the absorbance at 517 nm by UV spectrometer.

Haemolysis assay

Human red blood cells (RBC) were isolated using the standard procedure [48] and diluted with 0.1 M phosphate buffer saline (PBS) (pH 7.2). To 0.5 mL of RBC solution, six different concentrations (25, 50, 75, 100, 250 and 500 μg/mL) of the Ni(II) complexes were added to test the toxicity of the complexes. 100% lysis was initiated by adding 500 μL of H_2O, which acted as a negative control. RBC samples without H_2O and the Ni(II) complexes acted as a positive control. All the samples were incubated at 37 °C

for 30 min and centrifuged at 3000 rpm. The supernatant was used to analyse the percentage of lysis based on the absorbance at 560 nm.

In vitro cytotoxicity evaluation by MTT assay

Cytotoxicity of the Ni(II) complexes was carried out on lung cancer (A549), human breast cancer (MCF7) and mouse fibroblasts (L929) cell lines. Cell viability was carried out using the MTT assay [49]. The lung adenocarcinoma (A549), human breast (MCF7) cells and mouse fibroblasts (L929) were plated separately in 96-well plates at a concentration of 1×10^5 cells/well. Complexes (**1**–**4**) of concentration ranging from 1 to 500 μM dissolved in DMSO were seeded to the wells. DMSO was used as the control. After 24 h, the wells were treated with 20 μL of MTT [5 mg/mL PBS] and incubated at 37 °C for 4 h. The purple formazan crystals formed were dissolved in 200 μL of DMSO. The absorbance of the solution was measured at a wavelength of 570 nm using a Beckmann Coulter Elisa plate. Triplicate samples were analysed for each experiment. The percentage inhibition was calculated using the formula

$$\frac{\text{Mean OD of the untreated cells control} - \text{Mean OD of the treated cells}}{\text{Mean OD of the untreated cells (control)}} \times 100.$$

Hoechst 33258 staining

Cell pathology was detected by staining the nuclear chromatin of trypsinized cells (4.0×10^4 mL^{-1}) with 1 μL of Hoechst 33258 (1 mg/mL) for 10 min at 37 °C. Staining of suspension cells with Hoechst 33258 was used to view apoptotic changes. A drop of cell suspension was placed on a glass slide and a coverslip was laid over to reduce light diffraction. At random, 300 cells were observed in a fluorescent microscope fitted with a 377–355-nm filter and observed at 400× magnification, and the percentage of cells reflecting pathological changes was calculated [50].

Results and discussion

Synthesis

The thiosemicarbazone ligands (L1–L4) were synthesized via the typical condensation route from 3-indole aldehyde and appropriate thiosemicarbazides in the presence of glacial acetic acid (Scheme 1). Subsequently, the Ni(II) complexes (**1**–**4**) were prepared by heating the corresponding ligand with $NiCl_2 \cdot 6H_2O$ (Scheme 2). The ligands and their Ni(II) complexes were characterized by elemental analyses and various spectroscopic techniques. The molecular structure of L3, L4, **2**, **3** and **4** was confirmed by single crystal X-ray diffraction study.

Spectroscopy

The electronic spectra of the ligands showed two bands around 262–265 and 329–341 nm, which correspond to π–π^* and n–π^* transitions, respectively. The spectra of the complexes exhibited three bands in DMF solvent. Two bands appeared around 271–288 and 328–392 nm correspond to intraligand transitions. The band in the region 408–416 nm was attributed to ligand-to-metal charge-transfer (LMCT) transitions which indicated the formation of the complexes [17].

In the FT-IR spectra of the ligands, three bands were observed for indole N–H, N–H (attached to azomethine) and N–H (attached to thiocarbonyl) in the range of 3448–3409, 3343–3300 and 3238–3169 cm^{-1}, respectively. The azomethine (C=N) and thiocarbonyl (C=S) stretching frequencies of the ligands were observed at 1567–1548 and 1299–1261 cm^{-1}, respectively. On complexation, there was a decrease in azomethine (1511–1500 cm^{-1}) and thiocarbonyl (1263–1243 cm^{-1}) stretching frequencies, which suggested the coordination of the ligands to Ni ion through azomethine nitrogen and thiocarbonyl sulphur [51].

In the ^1H NMR spectra of the ligands, H–N–C=S proton resonated in the region 11.63–11.18 ppm. However, in

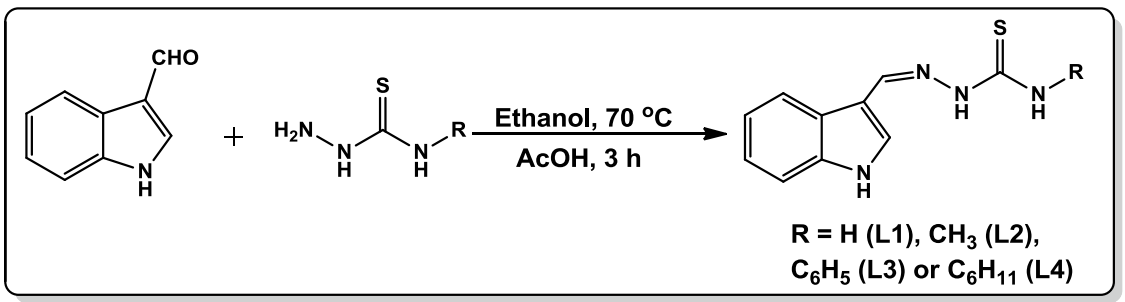

Scheme 1 Synthetic route of indole-based *N*-substituted thiosemicarbazone ligands

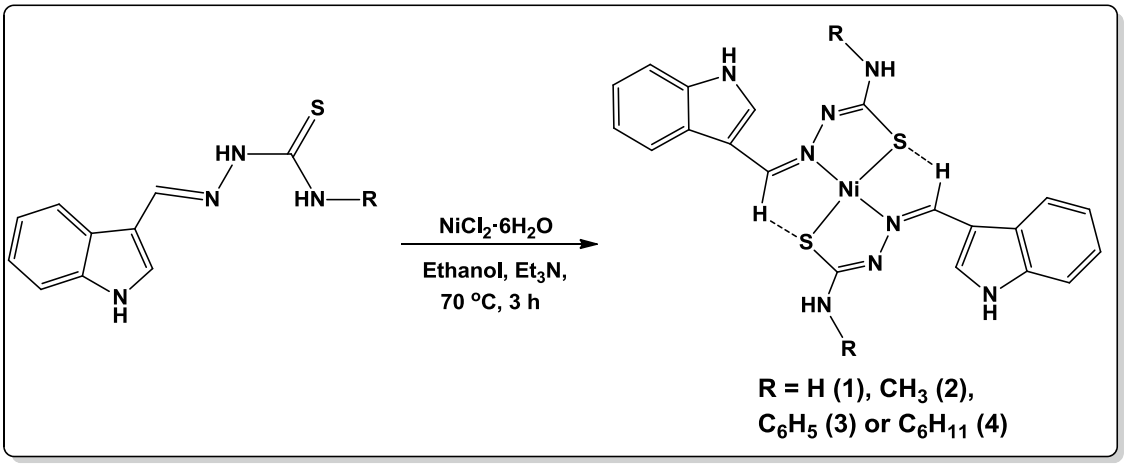

Scheme 2 Synthetic scheme of Ni(II) complexes

the spectra of the complexes (**1**–**4**), there was no resonance attributable to H–N–C=S, indicating the coordination of the ligands in the anionic form after deprotonation. The terminal N–H proton signal in the spectra of the ligands (L2–L4) and complexes was observed at 9.65–7.92 and 9.56–7.89 ppm, respectively. Two broad singlets were observed in the spectrum of L1 at 7.80 and 8.02 ppm corresponding to NH_2 protons. In the spectrum of **1**, one broad singlet was observed at 6.92 ppm corresponding to NH_2 protons of the coordinated ligand. The signal of indole N–H proton in the ligands and complexes appeared at 11.72–11.61 and 12.17–11.92 ppm, respectively. The signals around 8.31–8.05 and 7.81–7.61 ppm in the spectra of the ligands correspond to azomethine CH and indole CH protons. In the spectra of the complexes, the azomethine CH and indole CH protons showed signals around 8.04–7.80 and 7.57–7.51 ppm, respectively. Further, a doublet was observed at 3.09 and 2.84 ppm in the spectra of L2 and **2**, respectively, which was attributed to the presence of terminal CH_3 protons. ^{13}C NMR spectra of the ligands showed resonances due to C=S and C=N carbons in the regions 177.1–174.1 and 140.9–139.3 ppm, respectively. However, in the spectra of the complexes (**1**–**4**), C–S (after enolization and deprotonation) and C=N chemical shifts were observed at 174.7–173.2 and 147.2–141.1 ppm, respectively. Chemical shift of all other protons and carbons was observed in the expected regions [52].

Single crystal X-ray crystallography

Thermal ellipsoid plot of the ligands (L3 and L4) and complexes (**2**, **3** and **4**) with the atomic labelling scheme is shown in Figs. 1 and 2. Crystal data and selected inter atomic bond lengths and angles are given in Tables 1, 2, S1 and S2. Colourless crystals of the ligands were grown by slow evaporation of acetonitrile–methanol (1:1) solutions of the ligands. Red or brown crystals of the complexes suitable for X-ray diffraction were obtained by slow evaporation of their dichloromethane–dimethyl formamide (2:1) solutions. The important torsional angles N(2)–N(3)–C(10)–S(1), N(2)–N(3)–C(10)–N(4), N(3)–N(2)–C(9)–C(7) and C(9)–N(2)–N(3)–C(10) in L3 are 176.72(11), 3.5(2), −177.02(13) and −162.50(14)°, and those in L4 are 174.65(11), −6.5(2), −177.53(13) and 174.37(14)° [53]. The S(1)–C(10), N(2)–C(9) and N(2)–N(3) bond lengths of L3/L4 are 1.6945/1.6935(16), 1.2890(2)/1.2835(19) and 1.3842(17)/1.3927(18) Å, respectively.

Complexes **2**, **3** and **4** crystallized in triclinic *P-1* space group with *Z* of 1 (**2** and **3**) or 2 (**4**). The X-ray structure of **2**, **3** and **4** showed a perfect square planar geometry with nitrogen and sulphur atoms coordinate to Ni ion in a *trans* fashion. One molecule of dimethyl formamide was found in the asymmetric unit of **2** and four molecules of the same solvent were found in the symmetric unit of **3**. Two intramolecular hydrogen bonds were present between the azomethine H and S, which was rarely observed. The perfect square planar geometry was also reflected by τ_4 parameter [54, 55]. τ_4 can be calculated using the formula $\tau_4 = [360° - (\alpha + \beta)]/141°$. The value of τ_4 ranges from 1.00 for a perfect tetrahedral geometry, since $360 - 2(109.5) = 141$, to zero for a perfect square planar geometry, since $360 - 2(180) = 0$. For the intermediate structure like trigonal pyramidal, τ_4 falls within the range of 0–1.00. In complexes **2**, **3** and **4**, the angles S(1)–Ni(1)–S(1)#1 and N(1)#1–Ni(1)–N(1) were 180° which revealed perfect square planar geometry. There was an increase in the C–N and C–S bond lengths and decrease in the N(2)–N(3) bond length in **2**, **3** and **4** compared to L1, L3 and L4, respectively, which clearly attested the coordination of the ligand to Ni ion through azomethine N and thiocarbonyl

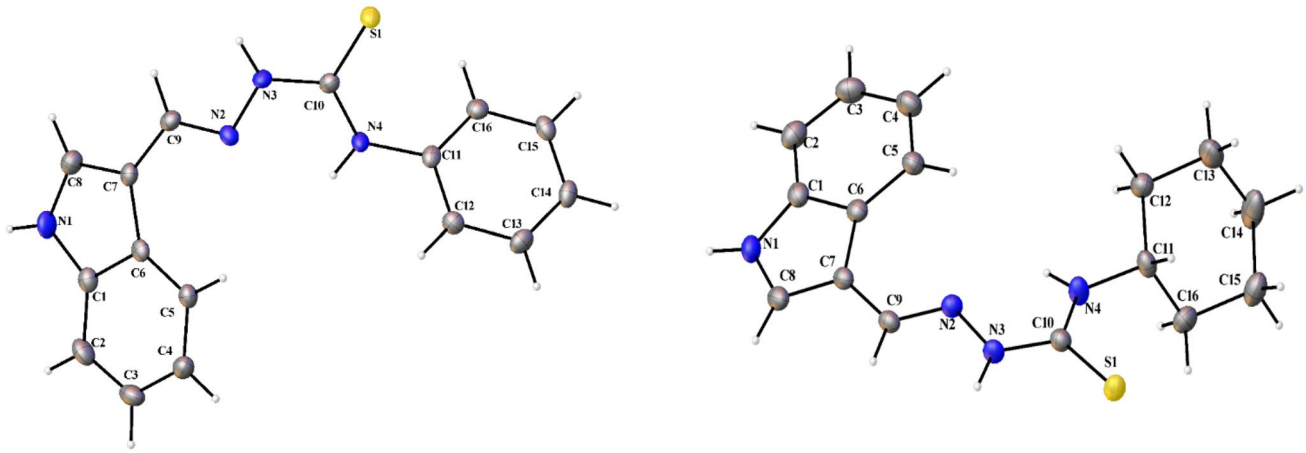

Fig. 1 Thermal ellipsoid plot of L3 and L4

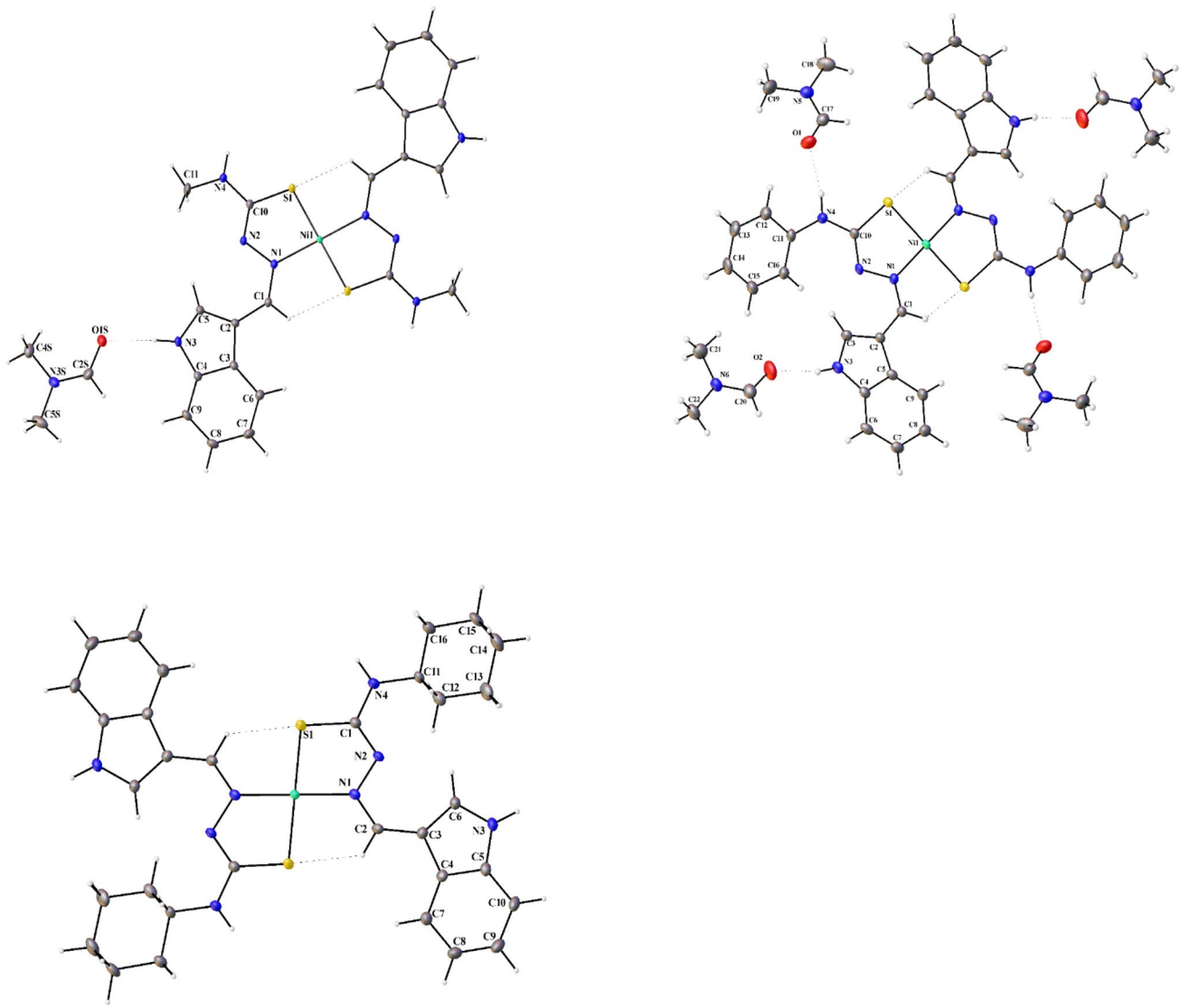

Fig. 2 Thermal ellipsoid plot of **2**, **3** and **4**

S after enolization and deprotonation. The Ni(1)–S(1) (2.161–2.176 Å) bond length is higher than Ni(1)–N(1) bond length (1.906–1.911 Å) in **2**, **3** and **4**. The torsional angles Ni(1)–S(1)–C(10/1)–N(2), Ni(1)–S(1)–C(10/1)–N(4), Ni(1)–N(1)–N(2)–C(10) and Ni(1)–N(1)–C(1/2)–C(2/3) in **2** are −13.30(12), 166.62(11), 16.17(14) and 174.64°(11), and those in **3** are 11.94(18), −169.99(14), −15.9(2) and 174.23°(16). 0.8(3), 180.0(2), 0.9(3) and −175.1°(2) are the values of the same torsional angles in **4**.

DNA binding studies

DNA binding is the predominant property looked for in pharmacology when evaluating the potential of new anticancer complexes, and hence, the interaction between DNA and the complexes needs to be investigated. The mode and tendency of the binding of complexes **1**–**4** with CT-DNA were studied with different methods.

Electronic absorption titration

Before performing DNA interaction studies, the stability of the complexes was verified in physiological medium (Tris–HCl buffer solution with a pH value of 7.2, containing 5% DMF) by UV–visible spectroscopic technique. There were no obvious changes in either the intensity or the position of the absorption bands in Tris–HCl buffer solution compared to those in DMF alone, which suggested that the complexes are stable under physiological conditions. The electronic spectra of Ni(II) complexes (**1**–**4**) in Tris–HCl buffer/5% DMF exhibited two bands around 273–284 and 333–391 nm, which correspond to intraligand transitions. The observation of changes in this band upon incremental addition of CT-DNA was used to find out the binding constant. Complexes binding to DNA through intercalation usually results in hypochromism with or without a small red or blue shift, since the intercalative mode involves a strong stacking interaction between the planar aromatic chromophore and the base pairs of DNA [56, 57]. The interaction of complexes **1**–**4** was confirmed by the observed hypochromism with red shift (Figs. 3, S1). The magnitude of hypochromism was in the order of **4** > **3** > **1** > **2**, which reflected the DNA binding affinities of the complexes. The intrinsic binding constant K_b was obtained from the ratio of slope to intercept in the plot of [DNA]/($\varepsilon_a - \varepsilon_f$) versus [DNA] according to the equation [58] [DNA]/($\varepsilon_a - \varepsilon_f$) = [DNA]/($\varepsilon_b - \varepsilon_f$) + 1/$K_b$ ($\varepsilon_b - \varepsilon_f$) where [DNA] is the concentration of DNA in base pairs, ε_a is the apparent extinction coefficient value found by calculating A(observed)/[complex], ε_f is the extinction coefficient for the free compound and ε_b is the extinction coefficient for the compound in the fully bound form. Each set of data, when fitted into the above equation, gave a straight line with a slope of 1/($\varepsilon_b - \varepsilon_f$) and an y-intercept of 1/K_b($\varepsilon_b - \varepsilon_f$) and the value of K_b was determined from the ratio of slope to intercept (Fig. 4a). The magnitudes of intrinsic binding constants (K_b) are given in Table 3. The K_b values were found to be in the range of 3.87×10^4–2.29×10^5 M^{-1}. The high binding ability of complex **4** compared to the other complexes might be due to the presence of cyclohexyl ring at the terminal nitrogen atom of the coordinated ligand [21].

EB displacement study

Fluorescence property has not been observed for the complexes at room temperature in solution or in the presence of CT-DNA. So the binding of the complexes with DNA could not be directly predicted through the emission spectra. Hence, competitive binding study was done to understand the mode of DNA interaction with the complexes [59–61]. EB is one of the most sensitive fluorescence probes that can bind with DNA [62]. The fluorescence of EB increases after intercalating into DNA. If the metal complex intercalates into DNA, it leads to a decrease in the binding sites of DNA available for EB, resulting in decrease in the fluorescence intensity of the CT-DNA–EB system [63]. The extent of decrease in the fluorescence intensity of CT-DNA–EB reflects the extent of interaction of the complex with CT-DNA. On adding the Ni(II) complexes (0–50 μM) to CT-DNA–EB, the quenching in the emission of DNA-bound EB took place (Figs. 3, S2) due to intercalation of the complexes with DNA. Fluorescence quenching is explained by the Stern–Volmer equation [64] $F°/F = 1 + K_q$ [Q] where $F°$ and F are the fluorescence intensities in the absence and presence of complex, respectively, K_q is a linear Stern–Volmer quenching constant, and [Q] is the concentration of complex. The slope of the plot of $F°/F$ versus [Q] gave K_q (Fig. 4a). The apparent DNA binding constant (K_{app}) values were calculated using the equation K_{EB} [EB] = K_{app} [complex] where [complex] is the complex concentration at 50% reduction in the fluorescence intensity of EB, $K_{EB} = 1.0 \times 10^7$ M^{-1} and [EB] = 5 μM. K_q and K_{app} values are listed in Table 3.

Viscosity measurements

Lengthening of DNA helix occurs on intercalation as base pairs are separated to accommodate the binding compound leading to increase in DNA viscosity. The values of relative specific viscosities of CT-DNA in the absence and presence of the compounds are plotted against [complex]/[DNA]. The relative viscosities of CT-DNA bound to the complexes (**1**–**4**) increased with increasing the compound concentration (Fig. 4b) similar to some known intercalators [65], indicative of a classical intercalation. The ability of

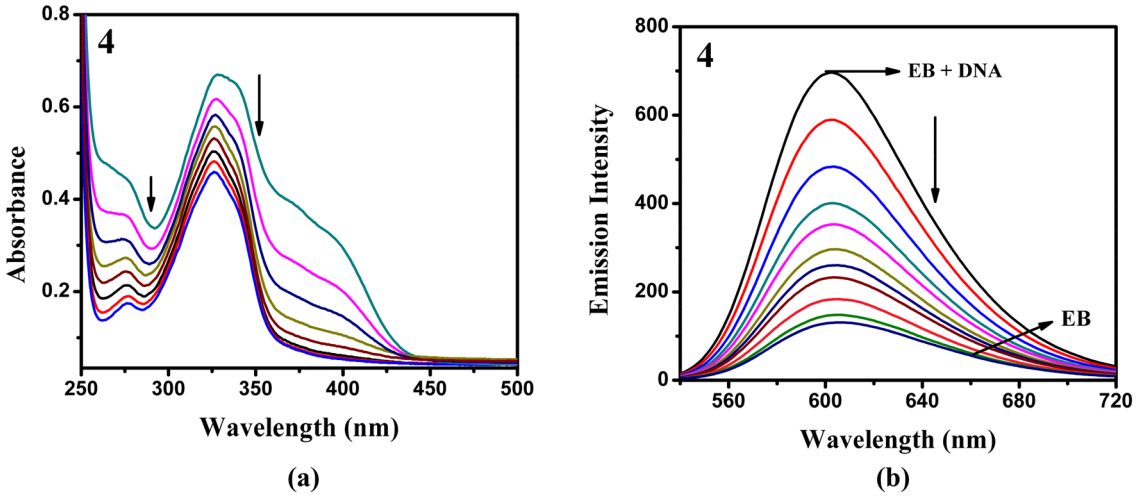

Fig. 3 **a** Absorption spectra of complex **4** in Tris–HCl buffer upon addition of CT-DNA. [Complex] = 20 μM, [DNA] = 0–35 μM. Arrow shows that the absorption intensity decreases upon increasing DNA concentration. **b** Fluorescence quenching curves of EB bound to DNA in the presence of **4**. [DNA] = 5 μM, [EB] = 5 μM and [complex] = 0–50 μM

the complexes to increase the viscosity of DNA followed the order **4** > **3** > **1** > **2**.

CD spectra

The CD spectrum of CT-DNA exhibited a positive band at 275 nm due to base stacking and a negative band at 245 nm due to helicity of B-DNA [66]. After the addition of **1**–**4**, the spectrum showed an increase in positive and a decrease in negative ellipticity with a red shift of 6–4 nm. These alterations in the CD spectrum of DNA indicated strong conformational changes by the complexes [67]. It was observed that complex **4** showed significant changes in the CD spectrum compared to the other complexes (Fig. 4c). Furthermore, the decrease in negative band is probably due to the unwinding of the DNA helix upon interaction with the complexes followed by transformation into A-like conformations [43, 68]. The CD results supported the order of binding ability of the complexes, obtained from other experiments.

Nuclease activity

To explore the DNA cleavage ability of the complexes (**1**–**4**), supercoiled (SC) pUC19 plasmid DNA (40 μM in base pairs) was incubated at 37 °C with the complexes (100 μM) in a 5% DMF/5 mM Tris–HCl/50 mM NaCl buffer at pH 7.2 for 4 h in the absence of external agent [69]. Complexes **1**–**4** cleaved SC (Form I) DNA into nicked circular (NC) (Form II) DNA (Fig. 4d), and the DNA cleavage strength follows the order **4** (92.3%) > **3** (52.6%) > **1** (38.2%) > **2** (1.7%). The study revealed that **4** cleaved DNA more efficiently than the other complexes, because of the strong partial intercalation of the cyclohexyl ring at the terminal nitrogen atom [70].

Protein binding studies

Fluorescence and absorbance quenching of BSA by the Ni(II) complexes

Fluorescence spectra are useful in the qualitative analysis of the binding of chemical compounds to BSA. Generally, the fluorescence of BSA is caused by two intrinsic characteristics of the protein, namely tryptophan and tyrosine. The intrinsic fluorescence of BSA will provide considerable information on their structure and dynamics and is often utilized in the study of protein folding and association reactions. The interaction of BSA with the complexes was studied by fluorescence measurement at room temperature. A solution of BSA (1 μM) was titrated with various concentrations of the complexes **1**–**4** (0–20 μM). Fluorescence spectra were recorded in the range of 290–500 nm upon excitation at 280 nm. The changes observed in the fluorescence emission spectra of BSA on addition of increasing concentration of the Ni(II) complexes are shown in Figs. 5a and S3. On the addition of complexes **1**–**4** to BSA, there was a significant decrease in the fluorescence intensity of BSA at 345 nm up to 75.23, 71.47, 85.62 and 78.01%, respectively, from the initial fluorescence intensity of BSA accompanied by a hypsochromic shift of 10–15 nm. The observed blue shift is mainly due to the fact that the active site in protein is buried in a hydrophobic environment. These results indicated a definite interaction of all of the complexes with the BSA protein [71, 72]. The fluorescence

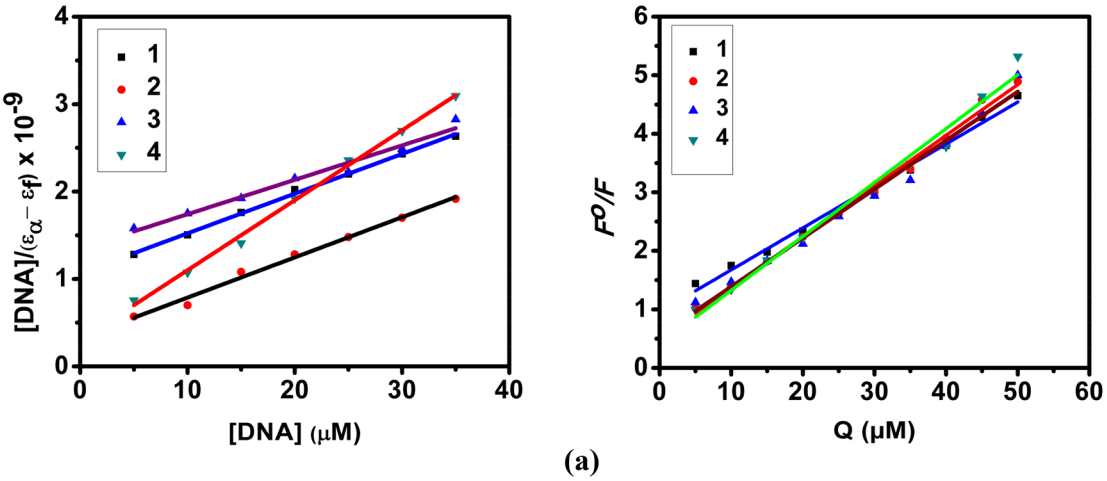

(a)

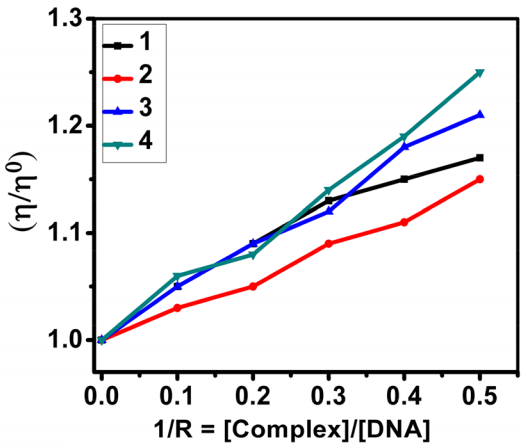

(b)

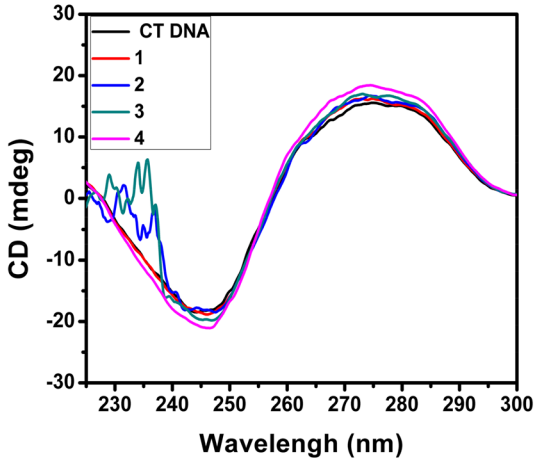

(c)

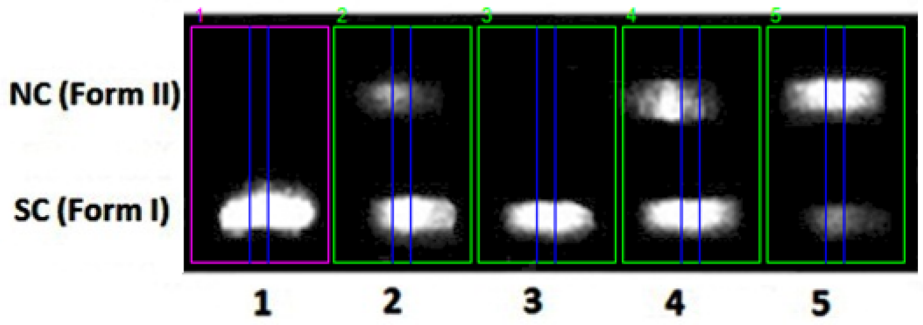

(d)

Fig. 4 **a** Plot of $[DNA]/(\varepsilon_a - \varepsilon_f)$ versus [DNA] and Stern–Volmer plot of fluorescence titrations of the complexes with CT-DNA. **b** Effect of the complexes (**1**, **2**, **3** and **4**) on the viscosity of CT-DNA. **c** CD spectra of CT-DNA (20 μM) in the absence and presence of 5 μM of the complexes. **d** Cleavage of supercoiled pUC19 DNA (40 μM) by complexes **1**–**4** in a buffer containing 5% DMF:5 mM Tris HCl/50 mM NaCl at pH = 7.2 and 37 °C with an incubation time of 4 h. *Lane 1* DNA control; *lane 2* DNA + **1** (100 μM); *lane 3* DNA + **2** (100 μM); *lane 4*, DNA + **3** (100 μM); *lane 5*, DNA + **4** (100 μM); forms SC and NC are supercoiled and nicked circular DNA, respectively

Table 3 DNA binding constant (K_b), quenching constant (K_q) and apparent binding constant (K_{app}) values

Complex	K_b (M^{-1})	K_q (M^{-1})	K_{app} (M^{-1})
1	4.25×10^4	8.62×10^4	4.31×10^6
2	3.87×10^4	7.16×10^4	3.58×10^6
3	1.95×10^5	9.20×10^4	4.60×10^6
4	2.29×10^5	9.82×10^4	4.91×10^6

quenching is described by the Stern–Volmer relation $F°/F = 1 + K_q$ [Q] where F^o and F demonstrate the fluorescence intensities in the absence and presence of quencher, respectively, K_q is a linear Stern–Volmer quenching constant, and [Q] is the quencher concentration. The quenching constant (K_q) can be calculated from the plot of $F°/F$ versus [Q] (Fig. 6a). When small molecules bind independently to a set of equivalent site, on a macromolecule, the equilibrium between free and bound molecules is represented by the Scatchard equation $\log[(F° - F)/F] = \log K_b + n \log [Q]$ where K_b is the binding constant of the complex with BSA and n is the number of binding site. From the plot of $\log [(F° - F)/F]$ versus $\log [Q]$ (Fig. 6a), the number of binding site (n) and the binding constant (K_b) values have been obtained. K_q, K_b and n values for the interaction of the Ni(II) complexes with BSA are provided in Table 4. The calculated value of n is around 1 for all of the compounds, indicating the existence of just a single binding site in BSA for all of the complexes. From the values of K_q and K_b, it was inferred that complex **4** interacted with BSA more strongly than the rest of the complexes. Here again, complex **4** showed better activity.

Quenching usually occurs either by dynamic or static mode. Dynamic quenching is a process in which the fluorophore and the quencher come into contact during the transient existence of the excited state. On the other hand,

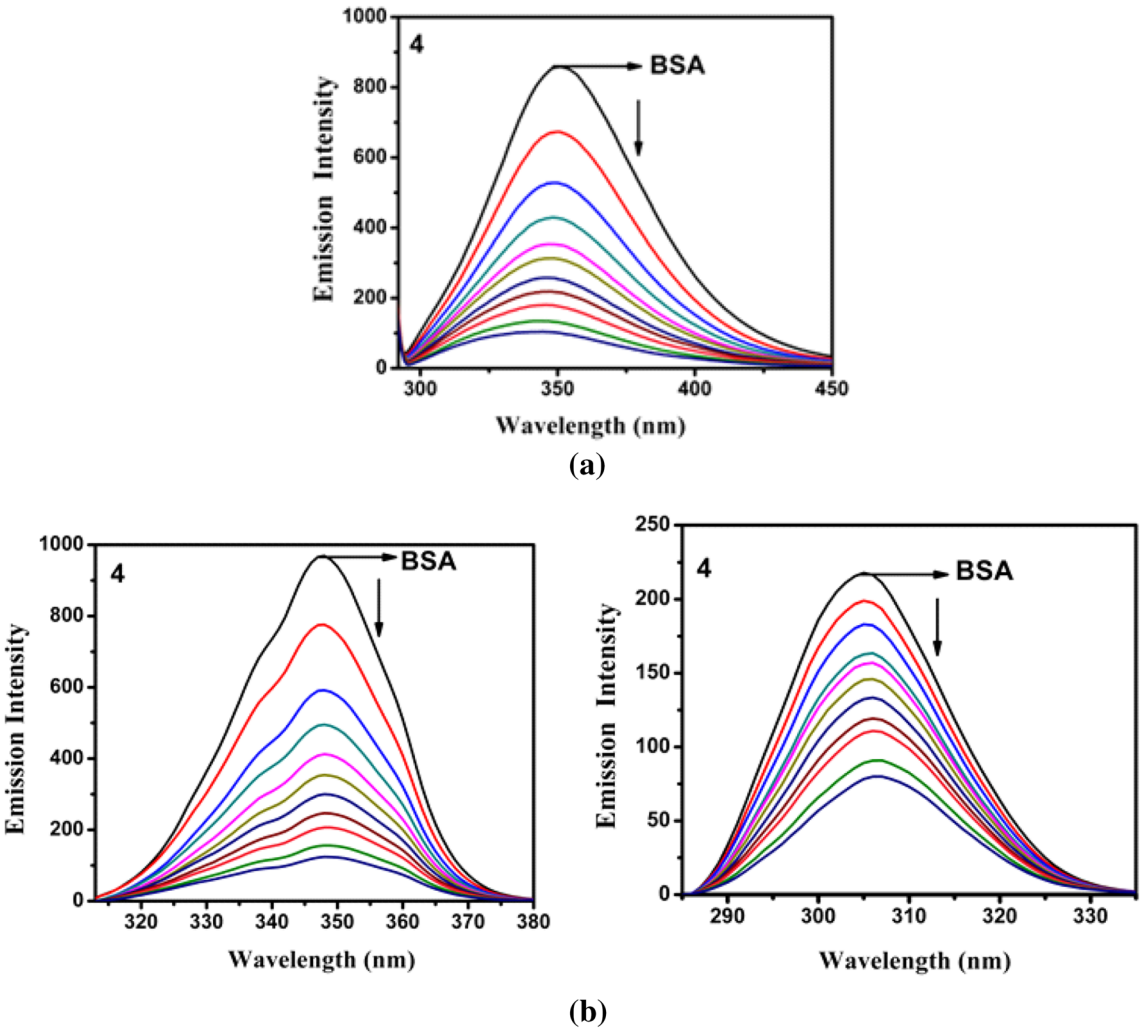

Fig. 5 **a** Fluorescence quenching curves of BSA in the absence and presence of **4**. [BSA] = 1 μM and [complex] = 0–20 μM. **b** Synchronous spectra of BSA (1 μM) as a function of concentration of **4** (0–20 μM) with $\Delta\lambda = 15$ and 60 nm

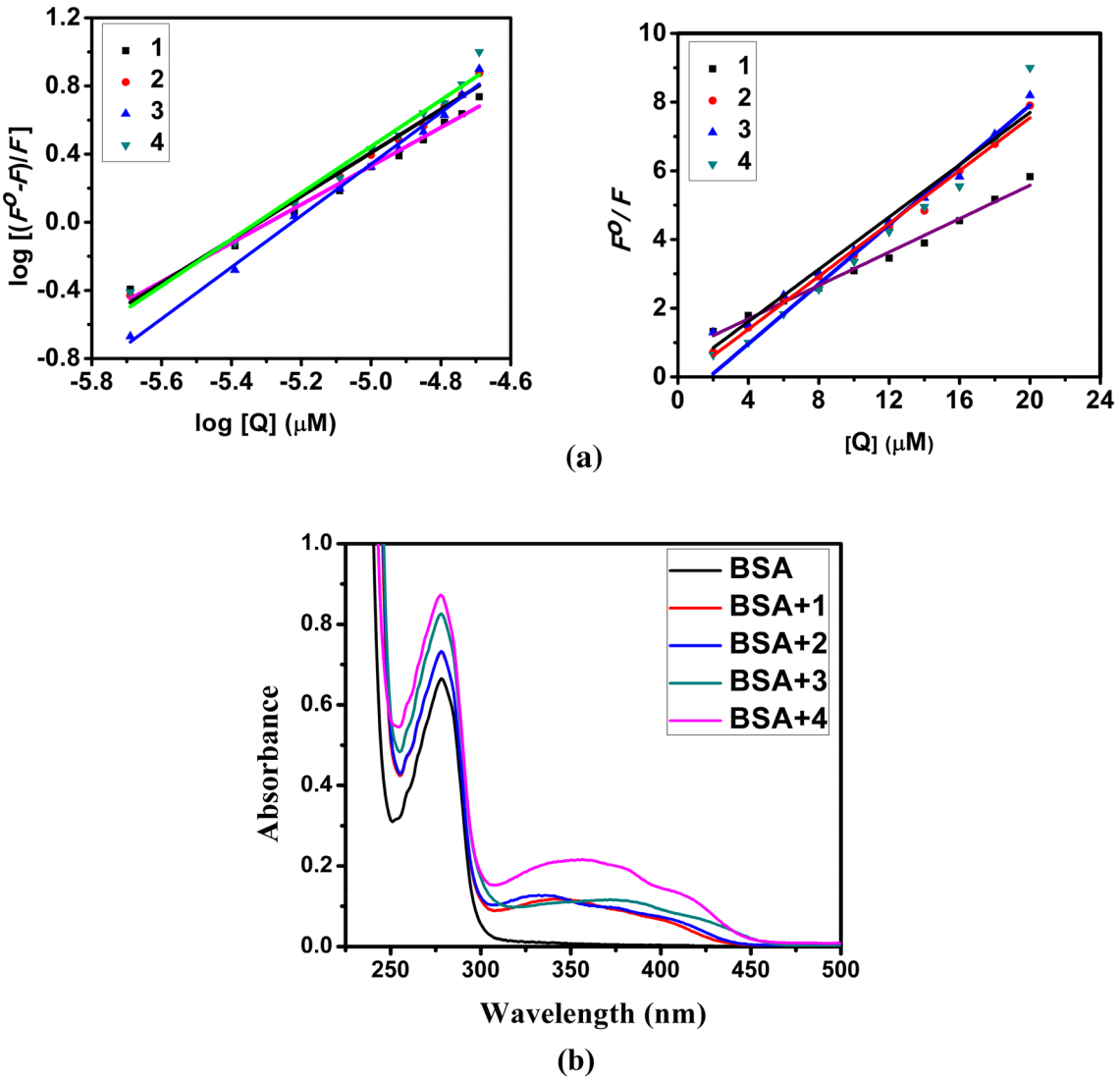

Fig. 6 **a** Stern–Volmer and Scatchard plots of the fluorescence titrations of the complexes with BSA. **b** The absorption spectra of BSA (10 μM) and BSA with **1**–**4** (5 μM)

static quenching refers to the formation of a fluorophore–quencher complex in the ground state [73]. A simple method to determine the type of quenching is UV–visible absorption spectroscopy. Addition of the complexes to BSA leads to an increase in BSA absorption intensity without affecting the position of absorption band (Fig. 6b). It showed the existence of static interaction between BSA and the complexes due to the formation of the ground-state complex as reported earlier [74].

Characteristics of synchronous fluorescence spectra

To investigate in detail the structural changes which occurred in BSA upon the addition of the new compounds, synchronous fluorescence spectra of BSA were measured before and after the addition of the test compounds. The results provided reasonable information on the molecular microenvironment, particularly in the vicinity of the fluorophore functional groups [74]. The difference between the excitation and emission wavelengths ($\Delta\lambda$) reflected the nature of the chromophore [62]. The large $\Delta\lambda$ value (60 nm) is characteristic of tryptophan residue and a small $\Delta\lambda$ value (15 nm) is characteristic of tyrosine. The synchronous fluorescence spectra of BSA with various concentrations of the complexes (**1**–**4**) were recorded at $\Delta\lambda$ = 15 and 60 nm. On addition of the complexes, the fluorescence intensity of tryptophan residue at 340 nm decreased in the magnitude of 76.9, 81.3, 79.7 and 71.6% for complexes **1**–**4**, respectively (Figs. 5b and S4). Similarly, there was also decrease in the intensity of tyrosine

Table 4 Protein binding constant (K_b), quenching constant (K_q) and number of binding site (n) values

Complex	K_b (M^{-1})	K_q (M^{-1})	n
1	9.98×10^5	3.93×10^5	1.19
2	9.05×10^5	2.43×10^5	1.13
3	1.81×10^6	4.56×10^5	1.03
4	2.57×10^6	4.92×10^5	1.10

residue at 300 nm. The magnitude of decrease was 70.1, 85.0, 80.6 and 87.9% for complexes **1**–**4**, respectively (Figs. 5b and S5). The synchronous fluorescence spectral studies clearly suggested that the fluorescence intensities of both the tryptophan and tyrosine were affected with increasing concentration of the complexes. The results indicated that the interaction of the complexes with BSA affected the conformation of both tryptophan and tyrosine micro-region [56].

Molecular docking with DNA and BSA

To gain insights into the possible reasons for the biological activity, the synthesized Ni(II) complexes were subjected to molecular docking studies using the AutoDock Tools (ADT) version 1.5.6 and AutoDock version 4.2.5.1 docking [75, 76]. In silico molecular docking studies were performed to simulate the interaction of the Ni complexes with the receptor binding site of B-DNA (PDB ID: 1BNA) dodecamer $d(CGCGAATTCGCG)_2$, human DNA topoisomerase I complex (DNA-T) (PDB ID: 1SC7) and BSA (PDB ID: 3V03) [77]. Docked conformation was analysed in terms of energy, hydrogen bonding and hydrophobic interactions between the Ni(II) complexes and receptors to find the binding nature of the potent inhibitors. The compound–DNA interactions were carried out with the detailed analysis, and final coordinates of the compound and receptor were saved. To display the interaction of the complexes with the receptor binding site, output was exported to PyMol software and detailed analysis was done, the free energy of binding (FEB) of the compounds was calculated from the docking scores and details are shown in Table 5.

In designing chemotherapeutic drugs, their interaction with DNA is vital to arrest the replication step in the cell cycle. DNA function can be suppressed in the physiological processes by the specific host–guest interaction between DNA and drugs. The metal complexes are widely used as the chemotherapeutic agents by destabilizing the DNA structure to block the cell functions.

We employed docking studies with the B-DNA (PDB ID: 1BNA) to predict the DNA binding affinity of the nickel(II) complexes. Ni(II) complexes **1**, **2**, **3** and **4** showed the binding energy values of −10.31, −9.72, −11.28, and −10.84 kcal/mol with two, four, three and three hydrogen bond interactions, respectively. Among all the complexes docked, **3** showed the lowest binding energy value of −11.28 kcal/mol with three hydrogen bonds with the docked DNA receptor. One of the phenyl attached N–H in **3** interacted with the oxygen of C=O of DT-20 and nitrogen of DA-6 to form two hydrogen bonds. Furthermore, indole N–H interacted with the oxygen of C=O of DT-8 and formed a hydrogen bond [78]. Interactions of all the Ni(II) complexes with the B-DNA receptor are shown in Fig S6. Docking studies revealed the efficient binding of the Ni(II) complexes with the DNA. This might disturb the stability of the DNA, which could trigger the DNA cleavage. Notably, molecular docking study was performed to predict the binding affinity and the sterically favourable conformations of the Ni(II) complexes towards DNA without considering the intercalation [79]. As molecular docking study considered only minor groove binding and experimental findings proposed intercalation of the complexes with DNA, no attempt was made to correlate the results of docking and experimental studies.

In the human DNA topoisomerase I complex (PDB ID: 1SC7), Topo-I was bound to the oligonucleotide sequence 50-AAAAAGACTTsX-GAAAATTTTT-30 in which 's' was 50-bridging phosphorothioate of the cleaved strand and 'X' represented any of the four bases A, G, C or T. The SH of G11 on the scissile strand was changed to OH and phosphoester bond of G12 in 1SC7 was rebuilt [80]. Molecular docking studies with DNA topoisomerase I clearly showed that the Ni(II) complexes approached towards the DNA cleavage site to form a stable complex which resulted in the binding energy between −9.29 and −12.80 kcal/mol

Table 5 Molecular docking parameters of complexes **1**–**4** with B-DNA (1BNA), DNA topoisomerase I (1SC7) and BSA (3V03)

Complex	Free energy of binding (kcal/mol)[a]		
	B-DNA (PDB ID: 1BNA)	DNA topoisomerase I (PDB ID: 1SC7)	BSA (PDB ID: 3V03)
1	−10.31	−9.29	−7.24
2	−9.72	−9.65	−7.36
3	−11.28	−12.15	−7.45
4	−10.84	−12.80	−8.07

[a] Calculated by Autodock

and subsequently leading to inhibitory effect. Among all the Ni(II) complexes docked, **4** showed the highest binding energy value of −12.80 kcal/mol with three hydrogen bonds with the docked 1SC7. In complex **4**, one of the indole N–H interacted through hydrogen bond with the pentose oxygen of DA-113 and C=O oxygen of ASN-722 amino acid. Binding interaction of the complexes with the DNA topoisomerase I receptor is shown in Fig. S7.

Docking studies of the complexes with 3V03 receptor showed that all the docked compounds bound efficiently with the receptor and exhibited free energy of binding value from −7.24 to −8.07 kcal/mol. The previously reported binding site in BSA was taken for this study [81]. All the Ni(II) complexes effectively bound in the 22 active site amino acids, namely PHE-205, ARG-208, ALA-209, LYS-211, TRP-213, VAL-215, PHE-227, THR-231, VAL-234, THR-235, ASP-323, LEU-326, GLY-327, LEU-330, SER-343, LEU-346, ALA-349, LYS-350, GLU-353, SER-479, LEU-480 and VAL-481. Among all the compounds docked with 3V03 receptor, compound **4** exhibited high binding; cyclohexyl attached N–H formed one hydrogen bond with ARG-208 amino acid, resulted in the binding energy of −8.07 kcal/mol. Binding interaction of the complexes with the BSA receptor is shown in Fig. S8.

Antioxidant activity

Reactive oxygen species cause oxidative damage to the cellular tissues and initiates various disorders. Due to this, there is an increasing interest in antioxidants, particularly in those intended to prevent the adverse effects of free radicals in the human body. In this regard, the Ni(II) complexes were studied for their antioxidant potential using DPPH scavenging assay. DPPH reacts with antioxidant compound which donates hydrogen and reduces the DPPH radical. The change in colour was measured at 517 nm. From the assay it was found that the IC_{50} value of **1** and **2** was about 75 µg/mL. The IC_{50} value of **3** and **4** was found to be 50 and 500 µg/mL, respectively. The results clearly showed that **3** was more potent radical scavenger compared to the other three complexes (**1**, **2** and **4**), which might be due to the electron withdrawing effect of the phenyl group on the terminal nitrogen atom [82]. The results are shown in Fig. S9.

Haemolysis assay

Ni(II) complexes (**1**–**4**) were tested for their toxicity against human RBC. From the results it was clearly inferred that the Ni(II) complexes (**1**–**4**) did not induce any haemolysis (Fig. S10). The results were compared to the control cells treated with water which produced 100% lysis. The results suggested that the Ni(II) complexes (**1**–**4**) could be used further as they did not show any toxicity against RBC [83].

In vitro cytotoxicity

The positive results obtained from the DNA and protein binding studies exhilarated us to test the cytotoxicity of the complexes (**1**–**4**). It was carried out against lung (A549) cancer, human breast (MCF7) cancer and mouse fibroblasts (L929) cell lines using MTT assay [84]. Figure S11 shows the cytotoxicity of the complexes (**1**–**4**) after 24 h incubation on A549, MCF7 and L929 cell lines, respectively. Complexes were dissolved in DMSO and a blank sample containing the same volume of DMSO was taken as a control to identify the activity of the solvent in this experiment. Cisplatin was used as a positive control to assess the cytotoxicity of the tested complexes. The results were analysed by means of cell inhibition expressed as IC_{50} values and are shown in Table 6. Figures S12 and S13 show digital images of the cancer cells (A549 and MCF7) and the cancer cells treated with the complexes (**1**–**4**). The IC_{50} values showed that complexes **4** and **1** exhibited higher inhibitory effect than that of the other complexes and the IC_{50} was close to that of cisplatin. Fortunately, all the complexes were less toxic towards the normal cell (L929) as it was evident from the higher IC_{50} values (600–750 µM) (Table 6). The cytotoxicity results are in good agreement with DNA binding ability of the complexes. Cytotoxicity of the nickel(II) complexes was compared with that of previously reported square planar nickel(II) complexes (Fig. 7). The present Ni(II) complexes showed higher activity than some of the other reported nickel(II) complexes. The cytotoxicity of nickel(II) complexes containing L-proline- and L-homoproline-4-*N*-pyrrolidine-3-thiosemicarbazone hybrid ligand showed IC_{50} value around 222.6 ± 17.1 µM against the A549 (96 h of incubation) cancer cell line [85]. The ionic square planar nickel complex bearing 4-chloro-5-methyl-salicylaldehyde thiosemicarbazone ligand showed higher cytotoxicity with lower IC_{50} (<10 µM) value against A549 (48 h of incubation) cancer cell line [16]. In vitro cytotoxicity of the Ni(II) complexes with substituted thiosemicarbazone ligands was good (IC_{50} = 25–30 µM) against human lung adenocarcinoma (A549) cell line, which was comparable with the

Table 6 In vitro cytotoxicity of the Ni(II) complexes in A549, MCF7 and L929 cell lines

Complex	IC_{50} (µM)		
	A549	MCF7	L929
1	52.4	125.1	>600
2	56.1	106.5	>700
3	57.2	62.0	>700
4	45.1	59.6	>750
Cisplatin	18.0	12.0	6.0

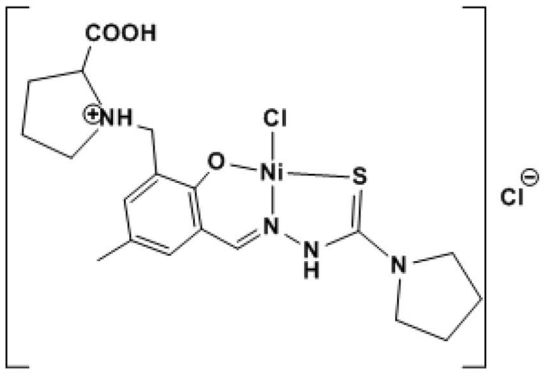

IC_{50} = 222.6 ± 17.1 μM
A549, 96 h of incubation

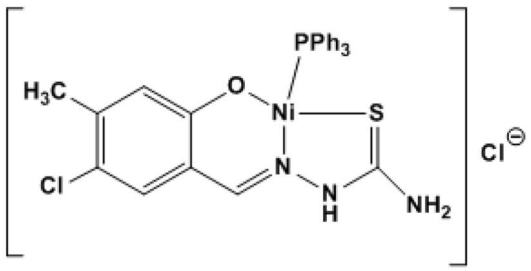

IC_{50} < 10 μM
A549, 48 h of incubation

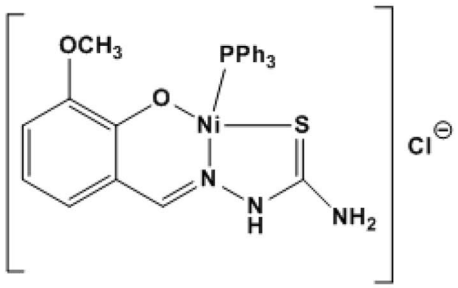

IC_{50} = 29 ± 1.02 μM
A549, 48 h of incubation

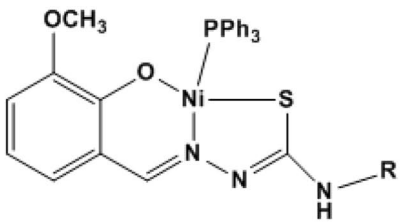

R = CH_3, C_2H_5 or C_6H_5
IC_{50} = 25-30 μM
A549, 48 h of incubation

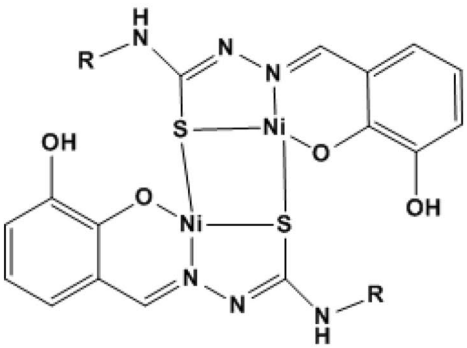

R = H, CH_3, C_6H_5 or C_2H_5
IC_{50} = 14.7-46.2 μM
MCF7, 48 h of incubation

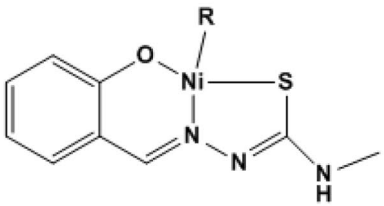

R = imidazole or benzimidazole
IC_{50} > 5 μM
MCF7

Fig. 7 IC_{50} values of reported square planar Ni(II) complexes

present results [86]. The complexes containing 2,3-dihydroxybenzaldehyde N4-substituted thiosemicarbazone ligands showed IC_{50} value around 14.7–46.2 μM against the MCF7 cell line [87]. The cytotoxicity of [Ni(MTSali)L] (MTSali = salicylaldehyde-4-methylthiosemicarbazone; L = imidazole or benzimidazole) type complexes against MCF7 cancer cell line is provided in Fig. 7 [88]. It is well evident from the comparison that our complexes showed high cytotoxicity. However, our complexes are less effective compared to cisplatin.

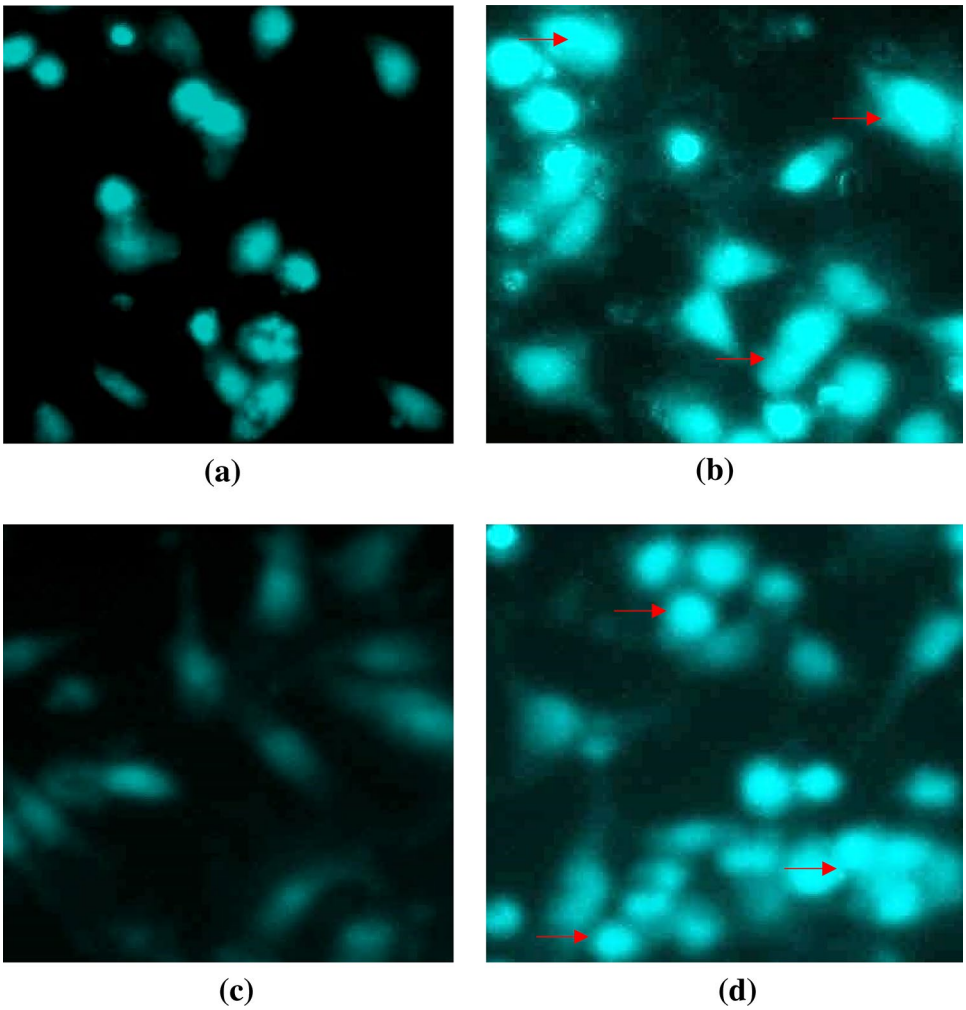

Fig. 8 Photomicrograph showing the features of Hoechst 33258 staining of A549 and MCF7 cancer cells. Cancer cells were treated with IC_{50} concentration of **4**. The cells were stained with Hoechst 33258 fluorescent dye: **a** untreated A549 cancer cells (control), **b** A549 cancer cells treated with **4** after 24 h. **c** MCF7 cancer cells (control), **d** MCF7 cancer cells treated with **4** after 24 h. Arrow marks indicate the apoptotic cells

Hoechst staining

Many antitumor agents used in chemotherapy are based on their ability to induce apoptosis in cancer cells [89, 90]. So the molecular mechanism of cell death has been studied by treating the complexes with the lung (A549) and human breast (MCF7) cancer cells. IC_{50} concentration of the Ni(II) complex (**4**) was used for the staining assay. The complex was incubated for 24 h and it was observed for cytological changes by adopting Hoechst 33258 staining. The results revealed that the cell death mechanism was apoptosis (Fig. 8) [91].

Conclusions

Four indole-based thiosemicarbazone ligands and their Ni(II) complexes were synthesized and characterized with a view to evaluate their biological applications. The complexes (**1**–**4**) bound to DNA via intercalation. Binding affinity of all the Ni(II) complexes with BSA was significant and the complexes bound to BSA in both tyrosine and tryptophan residues. The docked models also confirmed the binding affinity of the Ni(II) complexes with targeted DNA/protein. In addition, the complexes possess significant antioxidant activity. The haemolysis results revealed that the Ni(II) complexes (**1**–**4**) could be used for further pharmacological studies. The complexes showed high cytotoxicity against human lung (A549) and human breast (MCF7) cancer cell lines. DNA/protein binding and DNA cleavage ability of the complexes followed the order **4** > **3** > **1** > **2**. Cytotoxic property of the complexes was in different order towards A549 and MCF7, but **4** exhibited pronounced activity against both the cell lines. The high cytotoxicity of **4** might be due to the presence of bulky substitution (cyclohexyl) at the terminal nitrogen atom of the ligand. But the activity of the complexes was less compared to cisplatin. It is a convincing factor that there are reports on complexes having higher IC_{50} values than cisplatin (in vitro) showed significant activity in vivo [92, 93]. Apoptosis mechanism for the cell death was also confirmed.

Acknowledgements JH thanks the University Grants Commission for the fellowship (F1-17.1/2012-13/RGNF-2012-13-ST-AND-18716).

References

1. Hambley TW (2007) Dalton Trans 43:4929–4937
2. Orvig C, Abrams M (1999) Chem Rev 99:2201–2203
3. Thompson KH, Orvig C (2006) Dalton Trans 14:761–764
4. Santini C (2010) Chem Rev 254:1179–1218
5. Reedijk J (2008) Macromol Symp 270:193–201
6. Fricker SP (2007) Dalton Trans 43:4903–4917
7. Beraldo H, Gambino D (2004) Mini Rev Med Chem 4:31–39
8. Abid M, Agarwal SM, Azam A (2008) Eur J Med Chem 43:2035–2039
9. Mahalingam V, Chitrapriya N, Fronczek FR, Natarajan K (2008) Polyhedron 27:2743–2750
10. Liu MC, Lin TS, Sartorelli AC (1992) J Med Chem 35:3672–3677
11. Dilovic I, Rubcic M, Vrdoljak V, Pavelic SK, Kralj M, Piantanida Cindric IM (2008) Bioorg Med Chem 16:5189–5198
12. Duffy KJ, Shaw AN, Delorme E, Dillon SB, Miller CE, Giampa L, Huang Y, Keenan RM, Lamb P, Liu N, Miller SG, Price AT, Rosen J, Smith H, Wiggall KJ, Zhang L, Luengo JI (2002) J Med Chem 45:3573–3575
13. Cowley AR, Dilworth JR, Donnelly PS, Labisbal E, Sousa A (2002) J Am Chem Soc 124:5270–5271
14. Prabhakaran R, Kalaivani P, Jayakumar R, Zeller M, Hunter AD, Renukadevi SV, Ramachandran E, Natarajan K (2011) Metallomics 3:42–48
15. Kalaivani P, Prabhakaran R, Dallemer F, Poornima P, Vaishnavi E, Ramachandran E, Padma VV, Renganathan R, Natarajan K (2012) Metallomics 4:101–113
16. Ramachandran E, Kalaivani P, Prabhakaran R, Rath NP, Brinda S, Poornima P, Padma VV, Natarajan K (2012) Metallomics 4:218–227
17. Kalaivani P, Prabhakaran R, Ramachandran E, Dallemer F, Paramaguru G, Renganathan R, Poornima P, Padma VV, Natarajan K (2012) Dalton Trans 4:2486–2499
18. Senthil Raja D, Bhuvanesh NSP, Natarajan K (2011) Inorg Chem 50:12852–12866
19. Oliveira RBD, Fagundes EMDS, Soares RPP, Andrade AA, Krettli AU, Zani CL (2008) Eur J Med Chem 43:1983–1988
20. Walcourt A, Loyevsky M, Lovejoy DB, Gordeuk VR, Richardson DR (2004) Int J Biochem Cell Biol 36:401–407
21. Ramachandran E, Senthil Raja D, Mike JL, Wagner TR, Zeller M, Natarajan K (2012) RSC Adv 2:8515–8525
22. Sundberg RJ (1996) Indoles. Academic Press, London
23. Bandini M, Eichholzer A (2009) Angew Chem Int Ed 48:9608–9644
24. Gillman PK, Bartlett JR, Bridges PK, Hunt A, Patel AJ, Kantamaneni BD, Curzon G (1981) J Neurochem 37:410–417
25. Higdon JV, Delage B, Williams DE, Dashwood RH (2007) Pharmacol Res 55:224–236
26. Yan XJ, Qi M, Telusma G, Yancopoulos S, Madaio M, Satoh M, Reeves WH, Teichberg S, Kohn N, Auborn K, Chiorazzi N (2009) Clin Immunol 131:481–494
27. Park N, Kim JK, Park WT, Cho JW, Lim YP, Park SU (2011) Mol Biol Rep 38:4947–4953
28. Chang X, Tou JC, Hong C, Kim HA, Riby JE, Firestone GL, Bjeldanes LF (2005) Carcinogenesis 26:771–778
29. Cope RB, Loehr C, Dashwood R, Kerkvliet NI (2006) Photochem Photobiol Sci 5:499–507
30. Dahlöf C (2005) Therapy 2:349–356
31. Behari J, Zeng G, Otruba W, Thompson M, Muller P, Micsenyi A, Sekhon S, Leoni L, Monga S (2007) J Hepatol 46:849–857
32. William H, Frishman MDN (1983) Engl J Med 308:940–945
33. APEX2 Program for data collection and integration on area detectors. BRUKER AXS Inc., Madison
34. SADABS, Sheldrick GM Program for absorption correction of area detector frames. BRUKER AXS Inc., Madison
35. Sheldrick GM (2008) Acta Cryst A64:112–122
36. Dolomanov OV, Bourhis LJ, Gildea RJ, Howard JAK, Puschmann H (2009) J Appl Cryst 42:339–341
37. Mitra K, Basu U, Khan I, Maity B, Kondaiah P, Chakravarty AR (2014) Dalton Trans 43:751–763
38. Simpson JA, Cheeseman KH, Smith SE, Dean RT (1988) Biochem J 54:519–523
39. Rajput C, Rutkaite R, Swanson L, Haq I, Thomas JA (2006) Chem Eur J 12:4611–4619
40. Cohen G, Eisenberg H (1969) Biopolymers 8:45–55
41. Deshpande MS, Kumbhar AA, Kumbhar AS, Kumbhakar M, Pal H, Sonawane UB, Joshi RR (2009) Bioconj Chem 20:447–459
42. Jeyalakshmi K, Haribabu J, Bhuvanesh NSP, Karvembu R (2016) Dalton Trans 45:12518–12531
43. Haribabu J, Jeyalakshmi K, Arun Y, Bhuvanesh NSP, Perumal PT, Karvembu R (2015) RSC Adv 5:46031–46049
44. Selvakumaran N, Bhuvanesh NSP, Karvembu R (2014) Dalton Trans 43:16395–16410
45. http://autodock.scripps.edu/resources/references
46. Oktay M, Gulein I, Kufreviolglu I, Labenson-Wiss U (2003) Technol 36:263–271
47. Haribabu J, Subhashree GR, Saranya S, Gomathi K, Karvembu R, Gayathri D (2015) J Mol Struct 1094:281–291
48. Yang ZG, Sun HX, Fang WH (2005) Vaccine 23:5196–5203
49. Mossman T (1983) J Immunol Methods 65:55–63
50. Stander A, Marais S, Stivaktas V (2009) J Ethnopharmacol 124:45–60
51. Prabhakaran R, Karvembu R, Hashimoto T, Shimizu K, Natarajan K (2005) Inorg Chim Acta 358:2093–2096
52. Kalaivani P, Umadevi C, Prabhakaran R, Dallemer F, Mohan PS, Natarajan K (2014) Polyhedron 80:97–105
53. Vimala G, Govindaraj J, Haribabu J, Karvembu R, Subbiah Pandi A (2014) Acta Cryst E70:o1151
54. Murrayrust P, Burgi HB, Dunitz JD (1975) J Am Chem Soc 97:921–922
55. Keinan S, Avnir D (2001) J Chem Soc Dalton Trans 6:941–947
56. Senthil Raja D, Paramaguru G, Bhuvanesh NSP, Reibenspies JH, Renganathan R, Natarajan K (2011) Dalton Trans 40:4548–4559
57. Liu ZC, Wang BD, Li B, Wang Q, Yang ZY, Li TR, Li Y (2010) Eur J Med Chem 45:5353–5361
58. Pyle AM, Rehmann JP, Meshoyrer R, Kumar CV, Turro NJ, Barton JK (1989) J Am Chem Soc 111:3051–3058
59. Jeyalakshmi K, Selvakumaran N, Bhuvanesh NSP, Sreekanth A, Karvembu R (2014) RSC Adv 4:17179–17195
60. Lakowicz JR, Webber G (1973) Biochemistry 12:4161–4170
61. Baguley BC, Lebret M (1984) Biochemistry 23:937–943
62. Nyarko E, Hanada N, Habib A, Tabata M (2004) Inorg Chim Acta 357:739–745
63. Lepecq JB, Paoletti C (1967) J Mol Biol 27:87–106
64. Jeyalakshmi K, Arun Y, Bhuvanesh NSP, Perumal PT, Sreekanth A, Karvembu R (2015) Inorg Chem Front 2:780–798
65. Kumar CV, Asuncion EH (1993) J Am Chem Soc 115:8547–8553
66. Ivanov VI, Minchenkova LE, Schyolkina AK, Poletayer AI (1973) Biopolymers 12:89–110
67. Tamilselvi P, Palaniandavar M (2002) Inorg Chim Acta 337:420–428
68. Krishnamoorthy P, Sathyadevi P, Butorac RR, Cowley AH, Bhuvanesh NSP, Dharmaraj N (2012) Dalton Trans 41:4423–4436

69. Goswami TK, Gadadhar S, Balaji B, Gole B, Karande AA, Chakravarty AR (2014) Dalton Trans 43:11988–11999
70. Liu J, Zheng WJ, Shi S, Tan CP, Chen JC, Zheng KC, Ji LN (2008) J Inorg Biochem 102:193–202
71. Raja DS, Bhuvanesh NSP, Natarajan K (2011) Eur J Med Chem 46:4584–4594
72. Ramachandran E, Thomas SP, Poornima P, Kalaivani P, Prabhakaran R, Padma VV, Natarajan K (2012) Eur J Med Chem 50:405–415
73. Bhattacharyya M, Chaudhuri U, Poddar RK (1990) Biochem Biophys Res Commun 167:1146–1153
74. Senthil Raja D, Bhuvanesh NSP, Natarajan K (2012) Dalton Trans 41:4365–4377
75. Sanner MF (1999) J Mol Graphics Mod 17:57–61
76. Morris GM, Huey R, Lindstrom W, Sanner MF, Belew RK, Goodsell DS, Olson AJ (2009) J Comput Chem 30:2785–2791
77. Protein Data Bank. http://www.rcsb.org/pdb
78. Gao E, Sun N, Zhang S, Ding Y, Qiu X, Zhan Y, Zhu M (2016) Eur J Med Chem 121:1–11
79. Icsel C, Yilmaz VT, Kaya Y, Samli H, Harrison WTA, Buyukgungor O (2015) Dalton Trans 44(15):6880–6895
80. Xiao XS, Antony S, Pommier Y, Cushman M (2005) J Med Chem 48:3231–3238
81. Sankareswari VG, Vinod D, Mahalakshmi A, Alamelu M, Kumaresan G, Ramaraj R, Rajagopal S (2014) Dalton Trans 43:3260–3272
82. Ramachandran E, Senthil Raja D, Bhuvanesh NSP, Natarajan K (2012) Dalton Trans 41:13308–13323
83. Haribabu J, Subhashree GR, Saranya S, Gomathi K, Karvembu R, Gayathri D (2016) J Mol Struct 1110:185–195
84. Blagosklonny M, EIdiery WS (1996) Int J Cancer 67:386–392
85. Dobrova A, Platzer S, Bacher F, Milunovic MNM, Dobrov A, Spengler G, Enyedy ÉA, Novitchid G, Arion VB (2016) Dalton Trans 45:13427–13439
86. Kalaivani P, Saranya S, Poornima P, Prabhakaran R, Dallemer F, Vijaya Padma V, Natarajan K (2014) Eur J Med Chem 82:584–599
87. Shawish HB, Paydar M, Looi CY, Wong YL, Movahed E, Abdul Halim SN, Wong WF, Mustafa MR, Jamil Maah M (2014) Transition Met Chem 39:81–94
88. Mazlan NA, Begum TS, Ravoof A, Edward R, Tiekink T, Mohamed Tahir MI, Veerakumarasivam A, Crouse KA (2014) Transition Met Chem 39:633–639
89. Komeda S, Lutz M, Spek AL, Yamanaka Y, Sato T, Chikuma M, Reedijk J (2002) J Am Chem Soc 124:4738–4746
90. Ghobrial IM, Witzig TE, Adjei AA (2005) CA Cancer J Clin 55:178–194
91. Ramakrishnan S, Shakthipriya D, Suresh E, Periasamy VS, Akbarsha MA, Palaniandavar M (2011) Inorg Chem 50:6458–6471
92. Busto N, Valladolid J, Martinez-Alonso M, Lozano HJ, Jalon FA, Manzano BR, Rodriguez AM, Carrion MC, Biver T, Leal JM, Espino G, Garcia B (2013) Inorg Chem 52:9962–9974
93. Caruso F, Monti E, Matthews J, Rossi M, Gariboldi MB, Pettinari C, Pettinari R, Marchetti F (2014) Inorg Chem 53:3668–3677